J Sci Comput
DOI 10.1007/s10915-011-9505-3

A New Class of High-Order Energy Stable Flux Reconstruction Schemes for Triangular Elements

P. Castonguay · P.E. Vincent · A. Jameson

Received: 22 December 2010 / Revised: 27 April 2011 / Accepted: 7 June 2011
© Springer Science+Business Media, LLC 2011

Abstract The flux reconstruction (FR) approach allows various well-known high-order schemes, such as collocation based nodal discontinuous Galerkin (DG) methods and spectral difference (SD) methods, to be cast within a single unifying framework. Recently, the authors identified a new class of FR schemes for 1D conservation laws, which are simple to implement, efficient and guaranteed to be linearly stable for all orders of accuracy. The new schemes can easily be extended to quadrilateral elements via the construction of tensor product bases. However, for triangular elements, such a construction is not possible. Since numerical simulations over complicated geometries often require the computational domain to be tessellated with simplex elements, the development of stable FR schemes on simplex elements is highly desirable. In this article, a new class of energy stable FR schemes for triangular elements is developed. The schemes are parameterized by a single scalar quantity, which can be adjusted to provide an infinite range of linearly stable high-order methods on triangular elements. Von Neumann stability analysis is conducted on the new class of schemes, which allows identification of schemes with increased explicit time-step limits compared to the collocation based nodal DG method. Numerical experiments are performed to confirm that the new schemes yield the optimal order of accuracy for linear advection on triangular grids.

Keywords High-order methods · Flux reconstruction · Nodal discontinuous Galerkin method · Triangular elements · Stability

1 Introduction

Unstructured high-order methods can potentially yield better accuracy and reduced computational costs when compared to low-order methods (order of accuracy ≤ 2), especially for problems with complex physics and geometry, such as the simulation of vortex dominated flows over flapping wings. However, existing high-order methods are generally less

P. Castonguay (✉) · P.E. Vincent · A. Jameson
Department of Aeronautics and Astronautics, Stanford University, Stanford, CA 94305, USA
e-mail: pcasto2@stanford.edu

Published online: 30 June 2011

robust and more complex to implement than their low-order counterparts. These issues have prevented their wide-spread use.

The most popular unstructured high-order scheme for aerodynamic simulations is arguably the discontinuous Galerkin (DG) method, which was originally proposed by Reed and Hill [19] in 1973, and for which the theoretical basis has been provided in a series of papers by Cockburn and Shu [3–7]. A simple and efficient variant of the DG method is the collocation based nodal DG approach, which is discussed in the recent textbook by Hesthaven and Warburton [9]. In a collocation based nodal DG approach, the solution is represented by Lagrange interpolation at a set of collocation points in each element, and the quadratures required by the DG method can be pre-integrated. A similar method is the spectral difference (SD) method, for which the foundation was first put forward by Kopriva and Kolias [15] under the name of "staggered grid Chebyshev multidomain" methods. In 2006, Liu, Vinokur and Wang [17] presented a more general formulation for both triangular and quadrilateral elements, which they named the spectral difference method. As in a collocation based nodal DG approach, SD schemes achieve high-order accuracy by locally approximating the solution using a high-order polynomial inside each cell. In recent years, the SD method has been successfully used to solve a wide variety of problems [2, 16, 24].

In 2007, Huynh [10] presented the flux reconstruction (FR) approach, which is simple to implement and capable of unifying several high-order methods, including the collocation based nodal DG method and the SD method (at least for linear advection). In 2009, Huynh [11] extended the flux reconstruction approach to diffusion problems. Utilizing the FR formulation of Huynh [10], Jameson [12] showed that, for 1D linear advection, a particular SD method is stable for all orders of accuracy in a norm of Sobolev type. Recently, this result has been extended by Vincent, Castonguay and Jameson [22] who identified an infinite range of linearly stable FR schemes in 1D, henceforth referred as 1D Vincent-Castonguay-Jameson-Huynh (VCJH) schemes. The 1D VCJH schemes are parameterized by a single scalar quantity, which if chosen judiciously, leads to the recovery of several well known numerical methods (including the collocation based nodal DG method and a particular SD method), as well as one other FR scheme that was previously found by Huynh to be stable [10].

Any 1D FR scheme can easily be extended to quadrilateral and hexahedral elements via the construction of tensor product bases as described by Huynh [10], and therefore the extension of 1D VCJH schemes to those elements is straightforward. The VCJH schemes thereby obtained have many desirable characteristics, namely they are simple to implement, unifying and also guaranteed to be linearly stable. Since numerical simulations over complicated geometries often require the computational domain to be tessellated with simplex elements, the development of an approach on simplex elements with similar characteristics as the 1D VCJH schemes is highly desirable. For simplex elements, the direct construction of a tensor product basis is not possible and therefore, an alternative formulation is required. In 2009, Wang and Gao [23] proposed the lifting collocation penalty (LCP) approach as an extension of the FR scheme to triangular elements, in which a correction field is used to correct the discontinuous flux divergence. The correction field is determined from a lifting operator and it is shown that collocation based nodal DG, spectral volume (SV) and SD schemes can be recovered. However, the LCP approach does not lend itself obviously to the identification of stable schemes. In this article, a new and simple extension of the FR approach to triangular elements is proposed and is then used to identify an infinite range of high-order schemes on triangular elements which are linearly stable for all orders of accuracy.

The article begins with a brief review of the FR approach and a presentation of the VCJH schemes in one dimension. Following this review, an extension of the FR scheme to triangular elements is proposed and a new class of energy stable FR schemes on triangles is

identified. A von Neumann stability analysis is then performed on the new class of schemes in order to identify schemes that provide increased explicit time-step limits compared to collocation based nodal DG methods. Finally, numerical experiments are conducted in order to investigate the accuracy and stability properties of the new energy stable schemes and conclusions are presented.

2 The Flux Reconstruction Method in 1D

In this section, a brief review of the FR approach in one dimension is presented. Consider solving the following 1D scalar conservation law

$$\frac{\partial u}{\partial t} + \frac{\partial f}{\partial x} = 0 \tag{2.1}$$

within an arbitrary periodic domain $\mathbf{\Omega}$, where x is a spatial coordinate, t is time, $u = u(x,t)$ is a conserved scalar quantity and $f = f(u)$ is the flux of u in the x direction. Furthermore, consider partitioning $\mathbf{\Omega}$ into N non-overlapping, conforming elements each denoted $\mathbf{\Omega}_n = \{x | x_n < x < x_{n+1}\}$ such that

$$\mathbf{\Omega} = \bigcup_{n=1}^{N} \mathbf{\Omega}_n. \tag{2.2}$$

Finally, having partitioned $\mathbf{\Omega}$ into separate elements, consider representing the exact solution u within each $\mathbf{\Omega}_n$ by a function denoted by $u_n^\delta = u_n^\delta(x,t)$ which is a polynomial of degree p within $\mathbf{\Omega}_n$ and zero outside the element. Similarly, consider representing the exact flux f within each $\mathbf{\Omega}_n$ by a function denoted $f_n^\delta = f_n^\delta(x,t)$ which is a polynomial of degree $p+1$ inside $\mathbf{\Omega}_n$ and identically zero outside the element. Thus, the total approximate solution $u^\delta = u^\delta(x,t)$ and the total approximate flux $f^\delta = f^\delta(x,t)$ over the domain $\mathbf{\Omega}$ can be written as

$$u^\delta = \sum_{n=1}^{N} u_n^\delta \approx u, \qquad f^\delta = \sum_{n=1}^{N} f_n^\delta \approx f.$$

In order to simplify the implementation, it is advantageous to transform each $\mathbf{\Omega}_n$ to a standard element $\mathbf{\Omega}_S = \{r | -1 \leq r \leq 1\}$ via the mapping

$$x = \Theta_n(r) = \left(\frac{1-r}{2}\right) x_n + \left(\frac{1+r}{2}\right) x_{n+1}, \tag{2.3}$$

which has the inverse

$$r = \Theta_n^{-1}(x) = 2\left(\frac{x - x_n}{x_{n+1} - x_n}\right) - 1. \tag{2.4}$$

Having performed such a transformation, the evolution of u_n^δ within any individual $\mathbf{\Omega}_n$ (and thus the evolution of u^δ within $\mathbf{\Omega}$) can be determined by solving the following transformed equation within the standard element $\mathbf{\Omega}_S$

$$\frac{\partial \hat{u}^\delta}{\partial t} + \frac{\partial \hat{f}^\delta}{\partial r} = 0, \tag{2.5}$$

where

$$\hat{u}^{\delta} = \hat{u}^{\delta}(r,t) = u_n^{\delta}(\Theta_n(r),t) \tag{2.6}$$

is a polynomial of degree p,

$$\hat{f}^{\delta} = \hat{f}^{\delta}(r,t) = \frac{f_n^{\delta}(\Theta_n(r),t)}{J_n}, \tag{2.7}$$

is a polynomial of degree $p+1$, and $J_n = (x_{n+1} - x_n)/2$.

The FR approach to solving (2.5) within the standard element $\mathbf{\Omega}_S$ consists of five stages. The first stage is to define a specific form for $\hat{u}^{\delta}$. To this end, it is assumed that values of $\hat{u}^{\delta}$ are known at a set of $p+1$ solution points inside $\mathbf{\Omega}_S$, with each point located at a distinct position r_i ($i = 0$ to p). Lagrange polynomials $l_i = l_i(r)$ defined as

$$l_i = \prod_{j=0, j\neq i}^{p} \left(\frac{r - r_j}{r_i - r_j} \right) \tag{2.8}$$

can then be used to construct the following expression for $\hat{u}^{\delta}$

$$\hat{u}^{\delta} = \sum_{i=0}^{p} \hat{u}_i^{\delta}\, l_i, \tag{2.9}$$

where $\hat{u}_i^{\delta} = \hat{u}_i^{\delta}(t)$ are the known values of $\hat{u}^{\delta}$ at the solution points r_i.

The second stage of the FR approach involves constructing a degree p polynomial $\hat{f}^{\delta D} = \hat{f}^{\delta D}(r,t)$, defined as the approximate transformed discontinuous flux within $\mathbf{\Omega}_S$. A collocation projection at the $p+1$ solution points is employed to obtain $\hat{f}^{\delta D}$, which can hence be expressed as

$$\hat{f}^{\delta D} = \sum_{i=0}^{p} \hat{f}_i^{\delta D}\, l_i \tag{2.10}$$

where the coefficients $\hat{f}_i^{\delta D} = \hat{f}_i^{\delta D}(t)$ are simply values of the transformed flux at each solution point r_i evaluated directly from the approximate solution. The flux $\hat{f}^{\delta D}$ is termed discontinuous since it is calculated directly from the approximate solution, which is in general piecewise discontinuous between elements.

The third stage of the FR approach involves calculating numerical interface fluxes at either end of the standard element $\mathbf{\Omega}_S$ (at $r = \pm 1$). In order to calculate these fluxes, one must first obtain values for the approximate solution at either end of the standard element via (2.9). Once these values have been obtained they can be used in conjunction with analogous information from adjoining elements to calculate numerical interface fluxes. The exact methodology for calculating such numerical interface fluxes will depend on the nature of the equations being solved. For example, when solving the Euler equations one may use a Roe type approximate Riemann solver [20], or any other two-point flux formula that provides for an upwind bias. In what follows the common numerical interface fluxes associated with the left and right hand ends of $\mathbf{\Omega}_n$ (and transformed appropriately for use in $\mathbf{\Omega}_S$) will be denoted $\hat{f}_L^{\delta I}$ and $\hat{f}_R^{\delta I}$ respectively.

The penultimate stage of the FR approach involves adding a degree $p+1$ transformed correction flux $\hat{f}^{\delta C} = \hat{f}^{\delta C}(r,t)$ to the approximate transformed discontinuous flux $\hat{f}^{\delta D}$, such that their sum equals the transformed numerical interface flux at $r = \pm 1$, yet follows

(in some sense) the approximate discontinuous flux within the interior of $\mathbf{\Omega}_S$. This step is critical since it enables inter-element coupling. In order to define $\hat{f}^{\delta C}$ such that it satisfies the above requirements, consider first defining degree $p+1$ correction functions $h_L = h_L(r)$ and $h_R = h_R(r)$ that approximate zero (in some sense) within $\mathbf{\Omega}_S$, as well as satisfying

$$h_L(-1) = 1, \qquad h_L(1) = 0, \tag{2.11}$$

$$h_R(-1) = 0, \qquad h_R(1) = 1, \tag{2.12}$$

and, based on symmetry considerations

$$h_L(r) = h_R(-r). \tag{2.13}$$

Equation (2.13) ensures that the left correction function is a mirror image of the right correction function, with respect to the center of the element ($r = 0$). A suitable expression for $\hat{f}^{\delta C}$ can now be written in terms of h_L and h_R as

$$\hat{f}^{\delta C} = (\hat{f}_L^{\delta I} - \hat{f}_L^{\delta D})h_L + (\hat{f}_R^{\delta I} - \hat{f}_R^{\delta D})h_R, \tag{2.14}$$

where $\hat{f}_L^{\delta D} = \hat{f}^{\delta D}(-1, t)$ and $\hat{f}_R^{\delta D} = \hat{f}^{\delta D}(1, t)$. Using this expression, a degree $p+1$ approximate total transformed flux $\hat{f}^{\delta} = \hat{f}^{\delta}(r, t)$ within $\mathbf{\Omega}_S$ can be constructed from the discontinuous and correction fluxes as follows

$$\hat{f}^{\delta} = \hat{f}^{\delta D} + \hat{f}^{\delta C} = \hat{f}^{\delta D} + (\hat{f}_L^{\delta I} - \hat{f}_L^{\delta D})h_L + (\hat{f}_R^{\delta I} - \hat{f}_R^{\delta D})h_R. \tag{2.15}$$

The final stage of the FR approach involves calculating the divergence of $\hat{f}^{\delta}$ at each solution point r_i using the expression

$$\frac{\partial \hat{f}^{\delta}}{\partial r}(r_i) = \sum_{j=0}^{k} \hat{f}_j^{\delta D} \frac{\mathrm{d}l_j}{\mathrm{d}r}(r_i) + (\hat{f}_L^{\delta I} - \hat{f}_L^{\delta D})\frac{\mathrm{d}h_L}{\mathrm{d}r}(r_i) + (\hat{f}_R^{\delta I} - \hat{f}_R^{\delta D})\frac{\mathrm{d}h_R}{\mathrm{d}r}(r_i). \tag{2.16}$$

Note that the symmetry condition (2.13) ensures that for identical corrections ($f^{\delta I} - f^{\delta D}$) at the left and right interfaces, the divergence of f^{δ} will also be symmetric with respect to the center of the element. These values can then be used to advance the approximate transformed solution $\hat{u}^{\delta}$ in time via a suitable temporal discretization of the following semi-discrete expression

$$\frac{\mathrm{d}\hat{u}_i^{\delta}}{\mathrm{d}t} = -\frac{\partial \hat{f}^{\delta}}{\partial r}(r_i). \tag{2.17}$$

The nature of a particular FR scheme depends solely on three factors, namely the location of the solution collocation points r_i, the methodology for calculating the transformed numerical interface fluxes $\hat{f}_L^{\delta I}$ and $\hat{f}_R^{\delta I}$, and finally the form of the flux correction functions h_L (and thus h_R). Huynh has shown that a collocation based (under integrated) nodal DG scheme is recovered in 1D if the corrections functions h_L and h_R are the right and left Radau polynomials respectively [10]. Huynh has also shown that SD type methods can be recovered (at least for a linear flux function) if the corrections h_L and h_R are set to zero at a set of p points within $\mathbf{\Omega}_S$ (located symmetrically about the origin) [10]. Huynh also suggested several additional forms of h_L (and thus h_R), leading to the development of new schemes, with various stability and accuracy properties. For further details of these new schemes see the article by Huynh [10].

3 Vincent-Castonguay-Jameson-Huynh Schemes in 1D

Recently, Vincent, Castonguay and Jameson [22] identified an infinite range of 1D FR schemes which are linearly stable for all orders of accuracy, henceforth be referred as 1D VCJH schemes. The 1D VCJH schemes can be recovered if the left and right corrections functions h_L and h_R are defined as

$$h_L = \frac{(-1)^p}{2}\left[\Psi_p - \left(\frac{\eta_p \Psi_{p-1} + \Psi_{p+1}}{1+\eta_p}\right)\right], \tag{3.1}$$

and

$$h_R = \frac{1}{2}\left[\Psi_p + \left(\frac{\eta_p \Psi_{p-1} + \Psi_{p+1}}{1+\eta_p}\right)\right], \tag{3.2}$$

where

$$\eta_p = \frac{\varepsilon(2p+1)(a_p p!)^2}{2}, \quad a_p = \frac{(2p)!}{2^p (p!)^2}, \tag{3.3}$$

Ψ_p is a Legendre polynomial of degree p, and ε is a free scalar parameter that must lie within the range

$$\frac{-2}{(2p+1)(a_p p!)^2} < \varepsilon < \infty. \tag{3.4}$$

Such correction functions satisfy

$$\int_{-1}^{1} h_L \frac{\partial \hat{u}^\delta}{\partial r} \mathrm{d}r - \varepsilon \left(\frac{\partial^p \hat{u}^\delta}{\partial r^p}\right)\left(\frac{\mathrm{d}^{p+1} h_L}{\mathrm{d}r^{p+1}}\right) = 0, \tag{3.5}$$

and

$$\int_{-1}^{1} h_R \frac{\partial \hat{u}^\delta}{\partial r} \mathrm{d}r - \varepsilon \left(\frac{\partial^p \hat{u}^\delta}{\partial r^p}\right)\left(\frac{\mathrm{d}^{p+1} h_R}{\mathrm{d}r^{p+1}}\right) = 0, \tag{3.6}$$

within the standard element $\mathbf{\Omega}_S$ for any transformed solution $\hat{u}^\delta$, and ensure that the resulting VCJH scheme will be linearly stable in the norm $\|u^\delta\|^{1D}_{p,2}$, defined as

$$\|u^\delta\|^{1D}_{p,2} = \left[\sum_{n=1}^{N} \int_{x_n}^{x_{n+1}} (u_n^\delta)^2 + \frac{\varepsilon}{2}(J_n)^{2p}\left(\frac{\partial^p u_n^\delta}{\partial x^p}\right)^2 \mathrm{d}x\right]^{1/2}. \tag{3.7}$$

It can be noted that several existing methods are encompassed by the class of VCJH schemes. In particular if $\varepsilon = \varepsilon_{dg} = 0$ then a collocation based nodal DG scheme is recovered. Alternatively, if

$$\varepsilon = \varepsilon_{sd} = \frac{2p}{(2p+1)(p+1)(a_p p!)^2}, \tag{3.8}$$

an SD method is recovered (at least for a linear flux function). It is in fact the only SD type scheme that can be recovered from the range of VCJH schemes. Furthermore, it is identical to the SD scheme that Jameson [12] proved to be linearly stable for all orders of accuracy. It

is also the only SD scheme that Huynh showed to be stable via Fourier analysis [10]. Finally, if

$$\varepsilon = \varepsilon_{hu} = \frac{2(p+1)}{(2p+1)p(a_p p!)^2}, \tag{3.9}$$

then a so called g_2 FR method is recovered, which was originally identified by Huynh [10] to be particularly stable. In fact, the linear combination (3.1) can alternatively be expressed as a combination of Radau polynomials, as was used by Huynh to construct two particular schemes which he found to be stable using Fourier analysis [11], and which are in the stable range defined by (3.4).

4 Extension of the Flux Reconstruction Approach to Triangles

In this section, a new, simple and intuitive extension of the FR approach to triangular elements is proposed, in which the correction functions lie in a Raviart-Thomas space. The resulting scheme is shown to be conservative.

4.1 Preliminaries

Consider the 2D scalar conservation law

$$\frac{\partial u}{\partial t} + \nabla_{xy} \cdot \mathbf{f} = 0 \tag{4.1}$$

within an arbitrary domain $\mathbf{\Omega}$, where x and y are spatial coordinates, t is time, $u = u(x, y, t)$ is a conserved scalar and $\mathbf{f} = (f, g)$ where $f = f(u)$ and $g = g(u)$ are the fluxes of u in the x and y directions respectively. Consider partitioning the domain $\mathbf{\Omega}$ into N non-overlapping, conforming linear triangular elements $\mathbf{\Omega}_n$ such that

$$\mathbf{\Omega} = \bigcup_{n=1}^{N} \mathbf{\Omega}_n. \tag{4.2}$$

Having partitioned $\mathbf{\Omega}$ into separate elements, consider representing the exact solution u within each $\mathbf{\Omega}_n$ by an approximate solution $u_n^\delta = u_n^\delta(x, y, t)$, which is a polynomial of degree p within $\mathbf{\Omega}_n$ and identically zero outside the element. Similarly, consider representing the exact flux $\mathbf{f}$ within each $\mathbf{\Omega}_n$ by a function $\mathbf{f}_n^\delta = (f_n^\delta, g_n^\delta) = \mathbf{f}_n^\delta(x, y, t)$, which is a polynomial within $\mathbf{\Omega}_n$ and identically zero outside the element. The total approximate solution $u^\delta = u^\delta(x, y, t)$ and a total approximate flux $\mathbf{f}^\delta = \mathbf{f}^\delta(x, y, t)$ can therefore be defined within $\mathbf{\Omega}$ as

$$u^\delta = \sum_{n=1}^{N} u_n^\delta \approx u, \qquad \mathbf{f}^\delta = \sum_{n=1}^{N} \mathbf{f}_n^\delta \approx \mathbf{f}. \tag{4.3}$$

To facilitate the implementation, each element $\mathbf{\Omega}_n$ in physical space is mapped to a reference equilateral triangle $\mathbf{\Omega}_S$ using a mapping $\mathbf{\Theta}_n$, as shown in Fig. 1. For a linear triangular element, the mapping $\mathbf{\Theta}_n$ is

$$\mathbf{x} = \mathbf{\Theta}_n(\mathbf{r}) = \frac{(-3r + 2 - \sqrt{3}s)}{6}\mathbf{x}_{1,n} + \frac{(2 + 3r - \sqrt{3}s)}{6}\mathbf{x}_{2,n} + \frac{(2 + 2\sqrt{3}s)}{6}\mathbf{x}_{3,n} \tag{4.4}$$

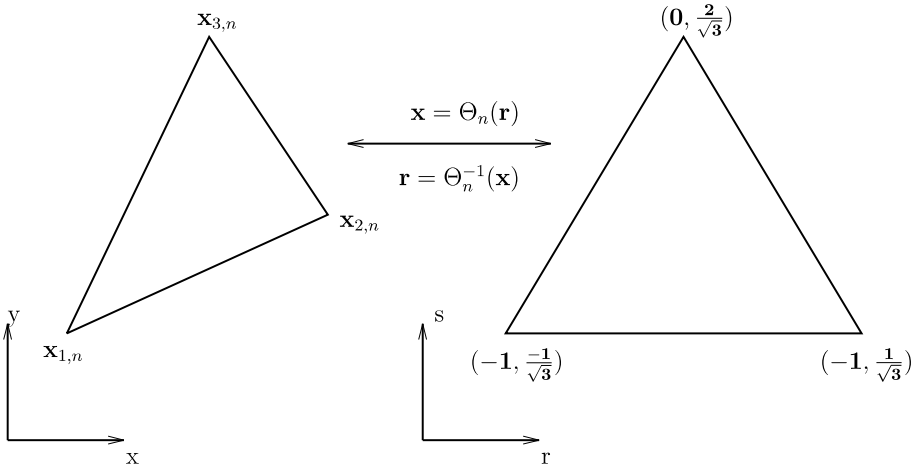

Fig. 1 Mapping between the physical space (x, y) and the computational space (r, s)

where $\mathbf{x}_{1,n}, \mathbf{x}_{2,n}$ and $\mathbf{x}_{3,n}$ are the coordinates of the vertices of the triangular element $\mathbf{\Omega}_n$ in physical space. The governing equation (4.1) in the physical domain can be transformed to the following equivalent governing equation in the reference domain

$$\frac{\partial \hat{u}}{\partial t} + \nabla_{rs} \cdot \hat{\mathbf{f}} = 0 \tag{4.5}$$

where

$$\hat{u} = Ju, \tag{4.6}$$

$$\hat{\mathbf{f}} = (\hat{f}, \hat{g}) = \left(\frac{\partial y}{\partial s} f - \frac{\partial x}{\partial s} g, -\frac{\partial y}{\partial r} f + \frac{\partial x}{\partial r} g \right), \tag{4.7}$$

$$J = \frac{\partial x}{\partial r} \frac{\partial y}{\partial s} - \frac{\partial x}{\partial s} \frac{\partial y}{\partial r}. \tag{4.8}$$

Hence, the evolution of u_n^δ within any individual $\mathbf{\Omega}_n$ (and thus the evolution of u^δ within $\mathbf{\Omega}$) can be determined by solving

$$\frac{\partial \hat{u}^\delta}{\partial t} + \nabla_{rs} \cdot \hat{\mathbf{f}}^\delta = 0 \tag{4.9}$$

where

$$\hat{u}^\delta = \hat{u}^\delta(\mathbf{r}, t) = J_n \, u_n^\delta(\mathbf{\Theta}_n(\mathbf{r}), t), \tag{4.10}$$

$$\hat{\mathbf{f}}^\delta = \hat{\mathbf{f}}^\delta(\mathbf{r}, t) = (\hat{f}^\delta, \hat{g}^\delta) \tag{4.11}$$

$$= \left(\frac{\partial y}{\partial s} f_n^\delta - \frac{\partial x}{\partial s} g_n^\delta, -\frac{\partial y}{\partial r} f_n^\delta + \frac{\partial x}{\partial r} g_n^\delta \right) \tag{4.12}$$

and the metric terms J_n, $\frac{\partial x}{\partial r}$, $\frac{\partial x}{\partial s}$, $\frac{\partial y}{\partial r}$ and $\frac{\partial y}{\partial s}$ (which depend on the shape of element n) can be evaluated from (4.4). For the transformation defined by (4.5) to (4.8), the following proper-

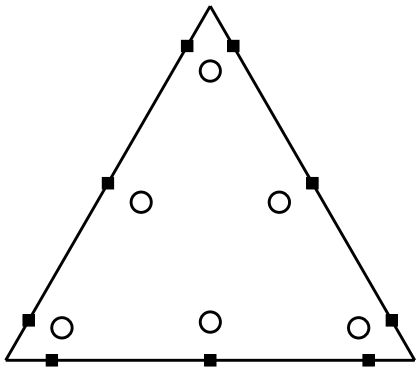

Fig. 2 Solution points (*circles*) and flux points (*squares*) in the reference element for $p = 2$. Flux points are located at Gauss points along each edge

ties hold

$$\nabla_{xy} \cdot \mathbf{f}_n^\delta = \frac{1}{J_n} \left(\nabla_{rs} \cdot \hat{\mathbf{f}}^\delta \right) \tag{4.13}$$

$$\int_{\mathbf{\Omega}_n} J_n u_n^\delta \, \nabla_{xy} \cdot \mathbf{f}_n^\delta \, d\mathbf{\Omega}_n = \int_{\mathbf{\Omega}_S} \hat{u}^\delta \, \nabla_{rs} \cdot \hat{\mathbf{f}}^\delta \, d\mathbf{\Omega}_S \tag{4.14}$$

$$\int_{\mathbf{\Gamma}_n} J_n u_n^\delta \, \mathbf{f}_n^\delta \cdot \mathbf{n} \, d\mathbf{\Gamma}_n = \int_{\mathbf{\Gamma}_S} \hat{u}^\delta \, \hat{\mathbf{f}}^\delta \cdot \hat{\mathbf{n}} \, d\mathbf{\Gamma}_S \tag{4.15}$$

where $\mathbf{\Gamma}_n$ and $\mathbf{\Gamma}_S$ refer to the boundary of the physical element $\mathbf{\Omega}_n$ and the reference element $\mathbf{\Omega}_S$, respectively.

Before the extension of the FR approach to triangular elements is presented, several definitions must be introduced. First, let $P_p(\mathbf{\Omega}_S)$ define the space of polynomial of degree $\leq p$ on $\mathbf{\Omega}_S$. The dimension of $P_p(\mathbf{\Omega}_S)$ is $\frac{1}{2}(p+1)(p+2)$. Furthermore, let the polynomial space $R_p(\mathbf{\Gamma}_S)$ on the edges of the reference element be defined as

$$R_p(\mathbf{\Gamma}_S) = \left\{ \phi \mid \phi \in L^2(\mathbf{\Gamma}_S), \;\; \phi|_{\mathbf{\Gamma}_f} \in P_p(\mathbf{\Gamma}_f), \;\; \forall \mathbf{\Gamma}_f \right\} \tag{4.16}$$

where $\mathbf{\Gamma}_f$ is used to represent edge f of the reference element $\mathbf{\Omega}_S$. Functions of $R_p(\mathbf{\Gamma}_S)$ are polynomials of degree $\leq p$ on each side of $\mathbf{\Omega}_S$, and are not necessarily continuous at the vertices.

Following the 1D FR approach, the approximate solution $\hat{u}^\delta$ within the reference element $\mathbf{\Omega}_S$ is represented by a multi-dimensional polynomial of degree p, defined by its values at a set of $N_p = \frac{1}{2}(p+1)(p+2)$ solution points (represented by hollow circles in Fig. 2).

The approximate solution in the reference element takes the form

$$\hat{u}^\delta(\mathbf{r}, t) = \sum_{i=1}^{Np} \hat{u}_i^\delta l_i(\mathbf{r}) \tag{4.17}$$

where $\hat{u}_i^\delta = J_n \cdot u^\delta(\Theta_n^{-1}(\mathbf{r}_i), t)$ is the value of $\hat{u}^\delta$ at the solution point i and $l_i(\mathbf{r})$ is the multi-dimensional Lagrange polynomial associated with the solution point i in the reference equilateral triangle $\mathbf{\Omega}_S$. The approximate solution $\hat{u}^\delta$ lies in the space $P_p(\mathbf{\Omega}_S)$. As in the 1D FR approach, the total transformed approximate flux $\hat{\mathbf{f}}^\delta = (\hat{f}^\delta, \hat{g}^\delta)$ is written as the sum of a discontinuous component $\hat{\mathbf{f}}^{\delta D}$ and a correction component $\hat{\mathbf{f}}^{\delta C}$,

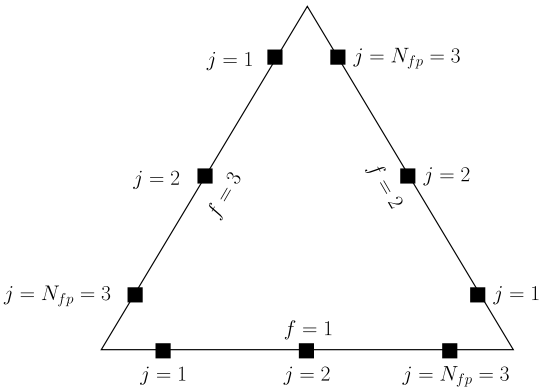

Fig. 3 Numbering convention for the faces and flux points on the reference triangular element. Example shown corresponds to $p = 2$. Flux points are located at Gauss points along each edge

$$\hat{\mathbf{f}}^{\delta} = \hat{\mathbf{f}}^{\delta D} + \hat{\mathbf{f}}^{\delta C}. \tag{4.18}$$

The transformed discontinuous flux $\hat{\mathbf{f}}^{\delta D} = (\hat{f}^{\delta D}, \hat{g}^{\delta D})$ is computed by constructing a degree p polynomial for each of its components as follows

$$\hat{f}^{\delta D} = \sum_{i=1}^{N_p} \hat{f}_i^{\delta D} l_i, \qquad \hat{g}^{\delta D} = \sum_{i=1}^{N_p} \hat{g}_i^{\delta D} l_i \tag{4.19}$$

where the coefficients $\hat{f}_i^{\delta D}$ and $\hat{g}_i^{\delta D}$ are the values of the transformed flux at the solution point i evaluated directly from the approximate solution $\hat{u}_i$ ($\hat{f}_i^{\delta D} = \hat{f}(\hat{u}_i)$ and $\hat{g}_i^{\delta D} = \hat{g}(\hat{u}_i)$). The divergence of the transformed discontinuous flux is therefore

$$\nabla_{rs} \cdot \hat{\mathbf{f}}^{\delta D} = \sum_{i=1}^{N_p} \hat{f}_i^{\delta D} \frac{\partial l_i}{\partial r} + \sum_{i=1}^{N_p} \hat{g}_i^{\delta D} \frac{\partial l_i}{\partial s}. \tag{4.20}$$

On each edge of the element, a set of $N_{fp} = (p + 1)$ flux points (illustrated by squares in Fig. 2) are defined and used to couple the solution between adjoining elements. The transformed correction flux $\hat{\mathbf{f}}^{\delta C}$ is constructed as follows

$$\hat{\mathbf{f}}^{\delta C}(\mathbf{r}) = \sum_{f=1}^{3} \sum_{j=1}^{N_{fp}} \left[(\hat{\mathbf{f}} \cdot \hat{\mathbf{n}})_{f,j}^{\delta I} - (\hat{\mathbf{f}}^{\delta D} \cdot \hat{\mathbf{n}})_{f,j} \right] \mathbf{h}_{f,j}(\mathbf{r}) \tag{4.21}$$

$$= \sum_{f=1}^{3} \sum_{j=1}^{N_{fp}} \Delta_{f,j} \mathbf{h}_{f,j}(\mathbf{r}). \tag{4.22}$$

Equations (4.21) and (4.22) deserve explanation. First, expressions subscripted by the indices f, j correspond to a quantity at the flux point j of face f, where $1 \leq f \leq 3$ and $1 \leq j \leq N_{fp}$. The convention used to number the faces and flux points is illustrated in Fig. 3.

For example, $(\hat{\mathbf{f}}^{\delta D} \cdot \hat{\mathbf{n}})_{f,j}$ is the normal component of the transformed discontinuous flux $\hat{\mathbf{f}}^{\delta D}$ at the flux point f, j. In (4.21), $(\hat{\mathbf{f}} \cdot \hat{\mathbf{n}})_{f,j}^{\delta I}$ is a normal transformed numerical flux computed at flux point f, j. As in the 1D FR method, it is computed by first evaluating the multiply defined values of u^{δ} at each flux point using (4.17). At each flux point, u_{-}^{δ} is defined as the

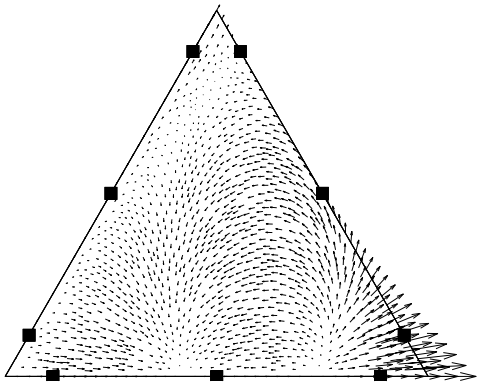

Fig. 4 Example of a vector correction function $\mathbf{h}_{f,j}$ associated with flux point $f = 2$, $j = 1$ for $p = 2$. Flux points are located at Gauss points along each edge

value of u^δ computed using the information local to the current element and u^δ_+ as the value of u^δ computed using information from the adjoining element that shares the same flux point. Once both approximate solution values (u^δ_- and u^δ_+) are evaluated at each flux point, a solver specific to the equations being solved is used to compute a common numerical flux $(\mathbf{f}\cdot\mathbf{n})^{\delta I}_{f,j}$ based on u^δ_+, u^δ_- and the local normal vector $\mathbf{n}_{f,j}$. From this common numerical flux, the normal transformed numerical flux denoted by $(\hat{\mathbf{f}}\cdot\hat{\mathbf{n}})^{\delta I}_{f,j}$ can be obtained. In (4.22), $\Delta_{f,j}$ is defined as the difference between the normal transformed numerical flux and the normal transformed discontinuous flux at the flux point f, j. Finally, $\mathbf{h}_{f,j}(\mathbf{r})$ is a vector correction function associated with flux point f, j. Each vector correction function $\mathbf{h}_{f,j}(\mathbf{r})$ is restricted to lie in the Raviart-Thomas space [18] of order p, denoted by $RT_p(\mathbf{\Omega}_S)$. Because of this property,

$$\begin{aligned} \nabla_{rs}\cdot\mathbf{h}_{f,j} &\in P_p(\mathbf{\Omega}_S) \\ \mathbf{h}_{f,j}\cdot\hat{\mathbf{n}}|_{\mathbf{\Gamma}_S} &\in R_p(\mathbf{\Gamma}_S) \end{aligned} \tag{4.23}$$

i.e. the divergence of each correction function ($\nabla_{rs}\cdot\mathbf{h}_{f,j}$) is a polynomial of degree $\leq p$ and the normal trace $\mathbf{h}_{f,j}\cdot\hat{\mathbf{n}}$ on $\mathbf{\Gamma}_S$ is also a polynomial of degree $\leq p$ along each edge. Furthermore, the correction functions $\mathbf{h}_{f,j}$ satisfy

$$\mathbf{h}_{f,j}(\mathbf{r}_{f_2,j_2})\cdot\hat{\mathbf{n}}_{f_2,j_2} = \begin{cases} 1 & \text{if } f = f_2 \text{ and } j = j_2 \\ 0 & \text{if } f \neq f_2 \text{ or } j \neq j_2 \end{cases} \tag{4.24}$$

An example of a vector correction function $\mathbf{h}_{f,j}$ is shown in Fig. 4 for the case $p = 2$.

It should be noted that because $\hat{\mathbf{f}}^{\delta D} \in P_p(\mathbf{\Omega}_S)$ and $P_p(\mathbf{\Omega}_S) \subset RT_p(\mathbf{\Omega}_S)$, then $\hat{\mathbf{f}}^{\delta D} \in RT_p(\mathbf{\Omega}_S)$. Furthermore, since each correction function $\mathbf{h}_{f,j} \in RT_p(\mathbf{\Omega}_S)$, (4.18) and (4.22) imply that

$$\hat{\mathbf{f}}^\delta \in RT_p(\mathbf{\Omega}_S) \tag{4.25}$$

and therefore

$$\hat{\mathbf{f}}^\delta\cdot\hat{\mathbf{n}}|_{\mathbf{\Gamma}_S} \in R_p(\mathbf{\Gamma}_S). \tag{4.26}$$

From (4.18), (4.22) and (4.24), it also follows that

$$\hat{\mathbf{f}}^{\delta C}(\mathbf{r}_{f,j})\cdot\hat{\mathbf{n}}_{f,j} = \left[(\hat{\mathbf{f}}\cdot\hat{\mathbf{n}})^{\delta I}_{f,j} - (\hat{\mathbf{f}}^{\delta D}\cdot\hat{\mathbf{n}})_{f,j}\right] = \Delta_{f,j} \tag{4.27}$$

and

$$\hat{\mathbf{f}}^{\delta}(\mathbf{r}_{f,j}) \cdot \hat{\mathbf{n}}_{f,j} = (\hat{\mathbf{f}} \cdot \hat{\mathbf{n}})^{\delta I}_{f,j} \tag{4.28}$$

at each flux point f, j. If one defines the polynomial function $l^{1D}_{f,j} \in R_p(\mathbf{\Gamma}_S)$ such that

$$l^{1D}_{f,j}(\mathbf{r}_{f_2,j_2}) = \begin{cases} 1 & \text{if } f = f_2 \text{ and } j = j_2 \\ 0 & \text{if } f \neq f_2 \text{ or } j \neq j_2 \end{cases} \tag{4.29}$$

then, the normal traces $\hat{\mathbf{f}}^{\delta C} \cdot \hat{\mathbf{n}}$ and $\hat{\mathbf{f}}^{\delta} \cdot \hat{\mathbf{n}}$ on $\mathbf{\Gamma}_S$ can be written as

$$\hat{\mathbf{f}}^{\delta C} \cdot \hat{\mathbf{n}}|_{\mathbf{\Gamma}_S} = \sum_{f=1}^{3} \sum_{j=1}^{N_{fp}} \Delta_{f,j} l^{1D}_{f,j} \tag{4.30}$$

and

$$\hat{\mathbf{f}}^{\delta} \cdot \hat{\mathbf{n}}|_{\mathbf{\Gamma}_S} = \sum_{f=1}^{3} \sum_{j=1}^{N_{fp}} (\hat{\mathbf{f}} \cdot \hat{\mathbf{n}})^{\delta I}_{f,j} l^{1D}_{f,j} \tag{4.31}$$

respectively. These properties of the approximate transformed flux $\hat{\mathbf{f}}^{\delta}$ will be useful when analysing the properties of the new approach in the following sections.

The correction field $\phi_{f,j}(\mathbf{r})$ is defined as the divergence of the correction function $\mathbf{h}_{f,j}(\mathbf{r})$, i.e.

$$\phi_{f,j}(\mathbf{r}) = \nabla_{rs} \cdot \mathbf{h}_{f,j}(\mathbf{r}). \tag{4.32}$$

Finally, combining (4.9), (4.18), (4.20) and (4.22), the approximate solution values at the solution points can be updated from

$$\frac{d\hat{u}^{\delta}_i}{dt} = -\left(\nabla_{rs} \cdot \hat{\mathbf{f}}^{\delta}\right)\Big|_{\mathbf{r}_i} \tag{4.33}$$

$$= -\left(\nabla_{rs} \cdot \hat{\mathbf{f}}^{\delta D}\right)\Big|_{\mathbf{r}_i} - \left(\nabla_{rs} \cdot \hat{\mathbf{f}}^{\delta C}\right)\Big|_{\mathbf{r}_i} \tag{4.34}$$

$$= -\sum_{k=1}^{N_p} \hat{f}^{\delta D}_k \frac{\partial l_k}{\partial r}\Big|_{\mathbf{r}_i} - \sum_{k=1}^{N_p} \hat{g}^{\delta D}_k \frac{\partial l_k}{\partial s}\Big|_{\mathbf{r}_i} - \sum_{f=1}^{3} \sum_{j=1}^{N_{fp}} \Delta_{f,j} \phi_{f,j}(\mathbf{r}_i). \tag{4.35}$$

The nature of a particular FR scheme on triangular elements depends on four factors, namely the location of the solution collocation points $\mathbf{r}_i$, the location of the flux points $\mathbf{r}_{f,j}$, the methodology for calculating the transformed numerical interface fluxes $(\hat{\mathbf{f}} \cdot \hat{\mathbf{n}})^{\delta I}_{f,j}$ and finally the form of the correction fields $\phi_{f,j}$.

4.2 Proof of Conservation

In order to prove that the extension of the FR scheme to triangular elements is locally conservative, the integral conservation law must be satisfied for each element of the domain. In other words, one must show that for all elements $\mathbf{\Omega}_n$ in the mesh,

$$\frac{d}{dt} \int_{\mathbf{\Omega}_n} u^{\delta}_n d\mathbf{\Omega}_n + \int_{\mathbf{\Gamma}_n} \mathbf{f}^{\delta}_n \cdot \mathbf{n}\, d\mathbf{\Gamma}_n = 0. \tag{4.36}$$

Consider transforming the first term on the left hand side of (4.36) to the reference space,

$$\frac{d}{dt}\int_{\mathbf{\Omega}_n} u_n^{\delta} d\mathbf{\Omega}_n = \frac{d}{dt}\int_{\mathbf{\Omega}_S} \frac{\hat{u}^{\delta}}{J} J\, d\mathbf{\Omega}_S = \frac{d}{dt}\int_{\mathbf{\Omega}_S} \hat{u}^{\delta} d\mathbf{\Omega}_S. \tag{4.37}$$

Because $\hat{u}^{\delta} \in P_p(\mathbf{\Omega}_S)$, it can be exactly integrated using a cubature rule associated with the N_p solution points. Hence,

$$\frac{d}{dt}\int_{\mathbf{\Omega}_S} \hat{u}^{\delta} d\mathbf{\Omega}_S = \frac{d}{dt}\sum_{i=1}^{Np} w_i \hat{u}_i^{\delta} \tag{4.38}$$

where w_i is the weight associated with the solution point i. Therefore, using (4.33), one obtains

$$\frac{d}{dt}\int_{\mathbf{\Omega}_S} \hat{u}^{\delta} d\mathbf{\Omega}_S = \frac{d}{dt}\sum_{i=1}^{Np} w_i \hat{u}_i^{\delta} = \sum_{i=1}^{Np} w_i \frac{d\hat{u}_i^{\delta}}{dt} = -\sum_{i=1}^{Np} w_i \left(\nabla_{rs}\cdot \hat{\mathbf{f}}^{\delta}\right)\Big|_{\mathbf{r}_i}. \tag{4.39}$$

Note that $(\nabla_{rs}\cdot \hat{\mathbf{f}}^{\delta})$ is also $\in P_p(\mathbf{\Omega}_S)$ and therefore,

$$-\sum_{i=1}^{Np} w_i \left(\nabla_{rs}\cdot \hat{\mathbf{f}}^{\delta}\right)\Big|_{\mathbf{r}_i} = -\int_{\mathbf{\Omega}_S} \left(\nabla_{rs}\cdot \hat{\mathbf{f}}^{\delta}\right) d\mathbf{\Omega}_S. \tag{4.40}$$

By transforming (4.40) back to physical space and integrating by parts, one obtains

$$-\sum_{i=1}^{Np} w_i \left(\nabla_{rs}\cdot \hat{\mathbf{f}}^{\delta}\right)\Big|_{\mathbf{r}_i} = -\int_{\mathbf{\Omega}_n} \left(\nabla_{xy}\cdot \mathbf{f}_n^{\delta}\right) d\mathbf{\Omega}_n = -\int_{\mathbf{\Gamma}_n} \mathbf{f}_n^{\delta}\cdot \mathbf{n}\, d\mathbf{\Gamma}_n. \tag{4.41}$$

Finally, combining (4.37), (4.39) and (4.41), one obtains

$$\frac{d}{dt}\int_{\mathbf{\Omega}_n} u_n^{\delta} d\mathbf{\Omega}_n + \int_{\mathbf{\Gamma}_n} \mathbf{f}_n^{\delta}\cdot \mathbf{n}\, d\mathbf{\Gamma}_n = 0 \tag{4.42}$$

thus proving local conservation of the scheme.

It follows from (4.26) that the normal trace $(\mathbf{f}^{\delta}\cdot\mathbf{n})$ of the total approximate flux $\mathbf{f}^{\delta}$ is a polynomial of degree p along each edge of $\mathbf{\Omega}_n$ and is therefore fully defined by its values of the numerical flux $(\mathbf{f}\cdot\mathbf{n})^{\delta I}$ at the $(p+1)$ flux points along each edge. Since at each edge flux point the numerical flux $(\mathbf{f}\cdot\mathbf{n})^{\delta I}$ is uniquely defined, and common to both cells sharing that edge, global conservation of the scheme follows.

5 Identification of Energy Stable Flux Reconstruction Schemes on Triangles

In this section, a class of energy stable FR schemes on triangles are identified. The section begins with a derivation of the criteria necessary to obtain energy stability. An infinite range of correction fields $\phi_{f,j}$ are then identified such that the aforementioned stability criteria are satisfied, and a methodology to enforce symmetry of the correction fields is presented. Finally, it is shown that the new family of energy stable FR schemes on triangles can recover the collocation based nodal DG method.

5.1 Preliminaries

First, let the operator $D^{(v,w)}$ be defined as

$$D^{(v,w)} = \frac{\partial^w}{\partial r^{(w-v+1)} \partial s^{(v-1)}} \tag{5.1}$$

where v and w are integers such that $1 \leq v \leq w+1$. For example,

$$D^{(1,2)} = \frac{\partial^2}{\partial r^2}, \qquad D^{(2,2)} = \frac{\partial^2}{\partial r \partial s}, \qquad D^{(3,2)} = \frac{\partial^2}{\partial s^2}. \tag{5.2}$$

On multiplying (4.34) by the multidimensional Lagrange polynomial $l_i(\mathbf{r})$ associated with solution point i, and summing over i (from 1 to N_p), one obtains

$$\sum_{i=1}^{N_p} \frac{d\hat{u}_i^\delta}{dt} l_i = -\sum_{i=1}^{N_p} \left(\nabla_{rs} \cdot \hat{\mathbf{f}}^{\delta D} \right) \Big|_{\mathbf{r}_i} l_i - \sum_{i=1}^{N_p} \left(\nabla_{rs} \cdot \hat{\mathbf{f}}^{\delta C} \right) \Big|_{\mathbf{r}_i} l_i \tag{5.3}$$

and thus

$$\frac{\partial \hat{u}^\delta}{\partial t} = -\left(\nabla_{rs} \cdot \hat{\mathbf{f}}^{\delta D} \right) - \left(\nabla_{rs} \cdot \hat{\mathbf{f}}^{\delta C} \right). \tag{5.4}$$

On multiplying (5.4) by $\hat{u}^\delta$, and integrating over $\mathbf{\Omega}_S$, one obtains

$$\frac{1}{2} \frac{\partial}{\partial t} \int_{\mathbf{\Omega}_S} (\hat{u}^\delta)^2 d\mathbf{\Omega}_S = -\int_{\mathbf{\Omega}_S} \hat{u}^\delta \left(\nabla_{rs} \cdot \hat{\mathbf{f}}^{\delta D} \right) d\mathbf{\Omega}_S - \int_{\mathbf{\Omega}_S} \hat{u}^\delta \left(\nabla_{rs} \cdot \hat{\mathbf{f}}^{\delta C} \right) d\mathbf{\Omega}_S. \tag{5.5}$$

Integrating the last term by parts, one obtains

$$\begin{aligned} \frac{1}{2} \frac{\partial}{\partial t} \int_{\mathbf{\Omega}_S} (\hat{u}^\delta)^2 d\mathbf{\Omega}_S = &- \int_{\mathbf{\Omega}_S} \hat{u}^\delta \left(\nabla_{rs} \cdot \hat{\mathbf{f}}^{\delta D} \right) d\mathbf{\Omega}_S \\ &- \int_{\mathbf{\Gamma}_S} \hat{u}^\delta \left(\hat{\mathbf{f}}^{\delta C} \cdot \hat{\mathbf{n}} \right) d\mathbf{\Gamma}_S \\ &+ \int_{\mathbf{\Omega}_S} \nabla_{rs} \hat{u}^\delta \cdot \hat{\mathbf{f}}^{\delta C} d\mathbf{\Omega}_S. \end{aligned} \tag{5.6}$$

Now, consider applying the operator $D^{(m,p)}$ to (5.4) for any integer m satisfying $1 \leq m \leq p+1$, thus obtaining

$$\frac{\partial}{\partial t} \left(D^{(m,p)} \hat{u}^\delta \right) = -D^{(m,p)} \left(\nabla_{rs} \cdot \hat{\mathbf{f}}^{\delta D} \right) - D^{(m,p)} \left(\nabla_{rs} \cdot \hat{\mathbf{f}}^{\delta C} \right). \tag{5.7}$$

Note that the discontinuous flux $\hat{\mathbf{f}}^{\delta D}$ is a vector whose components are polynomials of order p, hence $\nabla_{rs} \cdot \hat{\mathbf{f}}^{\delta D} \in P_{p-1}(\mathbf{\Omega}_S)$ which implies that

$$D^{(m,p)} \left(\nabla_{rs} \cdot \hat{\mathbf{f}}^{\delta D} \right) = 0. \tag{5.8}$$

Equation (5.7) then becomes

$$\frac{\partial}{\partial t} \left(D^{(m,p)} \hat{u}^\delta \right) = -D^{(m,p)} \left(\nabla_{rs} \cdot \hat{\mathbf{f}}^{\delta C} \right) \tag{5.9}$$

which is true for every m such that $1 \leq m \leq p+1$. On multiplying (5.9) by $D^{(m,p)}\hat{u}^{\delta}$ and integrating over the reference element, one obtains

$$\frac{1}{2}\frac{d}{dt}\int_{\mathbf{\Omega}_S}\left(D^{(m,p)}\hat{u}^{\delta}\right)^2 d\mathbf{\Omega}_S = -\int_{\mathbf{\Omega}_S}\left(D^{(m,p)}\hat{u}^{\delta}\right)\left(D^{(m,p)}\left(\nabla_{rs}\cdot\hat{\mathbf{f}}^{\delta C}\right)\right)d\mathbf{\Omega}_S \tag{5.10}$$

$$= -\sum_{f=1}^{3}\sum_{j=1}^{N_{fp}}\Delta_{f,j}\int_{\mathbf{\Omega}_S}\left(D^{(m,p)}\hat{u}^{\delta}\right)\left(D^{(m,p)}\phi_{f,j}\right)d\mathbf{\Omega}_S. \tag{5.11}$$

Since, $\hat{u}^{\delta}$ and $\phi_{f,j}$ are both $\in P_p(\mathbf{\Omega}_S)$, $D^{(m,p)}\hat{u}^{\delta}$ and $D^{(m,p)}\phi_{f,j}$ are constants and (5.11) simplifies to

$$\frac{1}{2}\frac{d}{dt}\int_{\mathbf{\Omega}_S}\left(D^{(m,p)}\hat{u}^{\delta}\right)^2 d\mathbf{\Omega}_S = -A_S\sum_{f=1}^{3}\sum_{j=1}^{N_{fp}}\Delta_{f,j}\left(D^{(m,p)}\hat{u}^{\delta}\right)\left(D^{(m,p)}\phi_{f,j}\right) \tag{5.12}$$

where A_S is the area of the reference equilateral triangle. Because (5.12) is true for every m such that $1 \leq m \leq p+1$, then

$$\frac{1}{2}\frac{d}{dt}\int_{\mathbf{\Omega}_S}\sum_{m=1}^{p+1}c_m\left(D^{(m,p)}\hat{u}^{\delta}\right)^2 d\mathbf{\Omega}_S = -A_S\sum_{f=1}^{3}\sum_{j=1}^{N_{fp}}\Delta_{f,j}\sum_{m=1}^{p+1}c_m\left(D^{(m,p)}\hat{u}^{\delta}\right)\left(D^{(m,p)}\phi_{f,j}\right) \tag{5.13}$$

for arbitrary scalar constants c_m. If every correction function $\mathbf{h}_{f,j}$, with its associated divergence $\phi_{f,j}$, satisfies

$$\sum_{m=1}^{p+1}c_m\left(D^{(m,p)}\hat{u}^{\delta}\right)\left(D^{(m,p)}\phi_{f,j}\right) = \int_{\mathbf{\Omega}_S}\mathbf{h}_{f,j}\cdot\nabla_{rs}\hat{u}^{\delta}\,d\mathbf{\Omega}_S \tag{5.14}$$

then (5.13) becomes

$$\frac{1}{2}\frac{d}{dt}\int_{\mathbf{\Omega}_S}\sum_{m=1}^{p+1}c_m\left(D^{(m,p)}\hat{u}^{\delta}\right)^2 d\mathbf{\Omega}_S = -A_S\sum_{f=1}^{3}\sum_{j=1}^{N_{fp}}\Delta_{f,j}\int_{\mathbf{\Omega}_S}\mathbf{h}_{f,j}\cdot\nabla_{rs}\hat{u}^{\delta}\,d\mathbf{\Omega}_S$$

$$= -A_S\int_{\mathbf{\Omega}_S}\hat{\mathbf{f}}^{\delta C}\cdot\nabla_{rs}\hat{u}^{\delta}\,d\mathbf{\Omega}_S. \tag{5.15}$$

Combining (5.15) and (5.6), one obtains

$$\frac{d}{dt}\int_{\mathbf{\Omega}_S}\left(\frac{(\hat{u}^{\delta})^2}{2}+\frac{1}{2A_S}\sum_{m=1}^{p+1}c_m\left(D^{(m,p)}\hat{u}^{\delta}\right)^2\right)d\mathbf{\Omega}_S$$

$$= -\int_{\mathbf{\Omega}_S}\hat{u}^{\delta}\left(\nabla_{rs}\cdot\hat{\mathbf{f}}^{\delta D}\right)d\mathbf{\Omega}_S - \int_{\mathbf{\Gamma}_S}\hat{u}^{\delta}\left(\hat{\mathbf{f}}^{\delta C}\cdot\hat{\mathbf{n}}\right)d\mathbf{\Gamma}_S. \tag{5.16}$$

Transforming to physical space, assuming linear elements (and thus a constant J_n), (5.16) becomes

$$\frac{d}{dt}\int_{\mathbf{\Omega}_n}\left(\frac{(u_n^{\delta})^2}{2}+\frac{1}{2A_S}\sum_{m=1}^{p+1}c_m\left(D^{(m,p)}u_n^{\delta}\right)^2\right)d\mathbf{\Omega}_n$$

$$= -\int_{\mathbf{\Omega}_n} u_n^{\delta} \left(\nabla_{xy} \cdot \mathbf{f}_n^{\delta D}\right) d\mathbf{\Omega}_n - \int_{\mathbf{\Gamma}_n} u_n^{\delta} \left(\mathbf{f}_n^{\delta C} \cdot \mathbf{n}\right) d\mathbf{\Gamma}_n. \tag{5.17}$$

The partial derivatives $D^{(m,p)}$ in transformed space can be transformed to partial derivatives in physical space using the chain rule and the mapping $\mathbf{\Theta}(\mathbf{r})$ defined in (4.4). Summing over all elements in the mesh, one obtains

$$\frac{d}{dt} \sum_{n=1}^{N} \left\{ \int_{\mathbf{\Omega}_n} \left(\frac{(u_n^{\delta})^2}{2} + \frac{1}{2A_S} \sum_{m=1}^{p+1} c_m \left(D^{(m,p)} u_n^{\delta}\right)^2 \right) d\mathbf{\Omega}_n \right\}$$
$$= \sum_{n=1}^{N} \left\{ -\int_{\mathbf{\Omega}_n} u_n^{\delta} \left(\nabla_{xy} \cdot \mathbf{f}_n^{\delta D}\right) d\mathbf{\Omega}_n - \int_{\mathbf{\Gamma}_n} u_n^{\delta} \left(\mathbf{f}_n^{\delta C} \cdot \mathbf{n}\right) d\mathbf{\Gamma}_n \right\}. \tag{5.18}$$

For constants c_m that satisfy

$$0 \le c_m < \infty \tag{5.19}$$

the expression

$$\left[\sum_{n=1}^{N} \int_{\mathbf{\Omega}_n} \left(\frac{(u_n^{\delta})^2}{2} + \frac{1}{2A_S} \sum_{m=1}^{p+1} c_m \left(D^{(m,p)} u_n^{\delta}\right)^2 \right) d\mathbf{\Omega}_n \right]^{1/2} \tag{5.20}$$

is a norm of the approximate solution u^{δ}, which will be denoted by $\|u^{\delta}\|_{p,2}$. Hence, (5.18) can be rewritten as

$$\frac{d}{dt} \|u^{\delta}\|_{p,2}^2 = \sum_{n=1}^{N} \left\{ -\int_{\mathbf{\Omega}_n} u_n^{\delta} \left(\nabla_{xy} \cdot \mathbf{f}_n^{\delta D}\right) d\mathbf{\Omega}_n - \int_{\mathbf{\Gamma}_n} u_n^{\delta} \left(\mathbf{f}_n^{\delta C} \cdot \mathbf{n}\right) d\mathbf{\Gamma}_n \right\}. \tag{5.21}$$

It will now be shown that the right hand side of (5.21) is guaranteed to be non-positive for the linear flux $\mathbf{f} = (au, bu)$ and for a common numerical flux computed from

$$(\mathbf{f} \cdot \mathbf{n})^{\delta I} = F(u_-, u_+, \mathbf{n}_-) = n_x \{\{au\}\} + n_y \{\{bu\}\} + \frac{\lambda}{2} |an_x + bn_y| [\![u]\!] \tag{5.22}$$

where

$$\{\{u\}\} = \frac{u_- + u_+}{2}, \qquad [\![u]\!] = u_- - u_+ \tag{5.23}$$

and $0 \le \lambda \le 1$ (with $\lambda = 0$ recovering a central scheme and $\lambda = 1$ recovering a fully upwind scheme). As mentioned earlier, the interior information of the element currently considered is represented by a subscript "$-$", the exterior information by a subscript "$+$" and in (5.22), n_x and n_y are the components of the outward pointing normal of the element currently considered (i.e. the components of $\mathbf{n}_-$). For the linear flux, $\mathbf{f} = (au, bu)$, the first term on the right hand side of (5.21) can be simplified as follows

$$\int_{\mathbf{\Omega}_n} u_n^{\delta} \left(\nabla_{xy} \cdot \mathbf{f}_n^{\delta D}\right) d\mathbf{\Omega}_n = \int_{\mathbf{\Omega}_n} u_n^{\delta} \left(\frac{\partial (au_n^{\delta})}{\partial x} + \frac{\partial (bu_n^{\delta})}{\partial y} \right) d\mathbf{\Omega}_n$$
$$= \frac{1}{2} \int_{\mathbf{\Omega}_n} \left(\frac{\partial (a(u_n^{\delta})^2)}{\partial x} + \frac{\partial (b(u_n^{\delta})^2)}{\partial y} \right) d\mathbf{\Omega}_n$$

$$= \frac{1}{2}\int_{\mathbf{\Gamma}_n} \left(a(u_n^\delta)^2 n_x + b(u_n^\delta)^2 n_y\right) d\mathbf{\Gamma}_n. \tag{5.24}$$

Using the definition of the transformed correction flux $\hat{\mathbf{f}}^{\delta C}$ given by (4.21), the second term on the right hand side of (5.21) becomes

$$\begin{aligned}\int_{\mathbf{\Gamma}_n} u_n^\delta \left(\mathbf{f}_n^{\delta C}\cdot\mathbf{n}\right) d\mathbf{\Gamma}_n &= \int_{\mathbf{\Gamma}_S} \frac{\hat{u}^\delta}{J_n}\left(\hat{\mathbf{f}}^{\delta C}\cdot\hat{\mathbf{n}}\right) d\mathbf{\Gamma}_S \\ &= \int_{\mathbf{\Gamma}_S} \frac{\hat{u}^\delta}{J_n}\left(\sum_{f=1}^{3}\sum_{j=1}^{N_{fp}}\left[(\hat{\mathbf{f}}\cdot\hat{\mathbf{n}})_{f,j}^{\delta I} - (\hat{\mathbf{f}}^{\delta D}\cdot\hat{\mathbf{n}})_{f,j}\right]\mathbf{h}_{f,j}\cdot\hat{\mathbf{n}}\right) d\mathbf{\Gamma}_S. \end{aligned}\tag{5.25}$$

From (4.23) and (4.24), the normal trace $\mathbf{h}_{f,j}\cdot\hat{\mathbf{n}}$ on $\mathbf{\Gamma}_S$ is a polynomial of degree p that takes the value of 1 at the flux point f, j and is zero at all other flux points. Hence, since the normal trace $\hat{\mathbf{f}}^{\delta D}\cdot\hat{\mathbf{n}}$ on $\mathbf{\Gamma}_S$ is also a polynomial of degree p, it is exactly represented by

$$\sum_{f=1}^{3}\sum_{j=1}^{N_{fp}}\left[(\hat{\mathbf{f}}^{\delta D}\cdot\hat{\mathbf{n}})_{f,j}\right]\mathbf{h}_{f,j}\cdot\hat{\mathbf{n}} \tag{5.26}$$

on $\mathbf{\Gamma}_S$, and therefore,

$$\begin{aligned}\int_{\mathbf{\Gamma}_S} \frac{\hat{u}^\delta}{J_n}\left(\sum_{f=1}^{3}\sum_{j=1}^{N_{fp}}\left[(\hat{\mathbf{f}}^{\delta D}\cdot\hat{\mathbf{n}})_{f,j}\right]\mathbf{h}_{f,j}\cdot\hat{\mathbf{n}}\right) d\mathbf{\Gamma}_S &= \int_{\mathbf{\Gamma}_S} \frac{\hat{u}^\delta}{J_n}\left(\hat{\mathbf{f}}^{\delta D}\cdot\hat{\mathbf{n}}\right) d\mathbf{\Gamma}_S \\ &= \int_{\mathbf{\Gamma}_n} u_n^\delta \left(\mathbf{f}_n^{\delta D}\cdot\mathbf{n}\right) d\mathbf{\Gamma}_n \\ &= \int_{\mathbf{\Gamma}_n} \left(a(u_n^\delta)^2 n_x + b(u_n^\delta)^2 n_y\right) d\mathbf{\Gamma}_n. \end{aligned}\tag{5.27}$$

Similarly, using the numerical flux function defined by (5.22), and because u^δ is a polynomial of degree p on $\mathbf{\Gamma}_S$,

$$\begin{aligned}&\int_{\mathbf{\Gamma}_S} \frac{\hat{u}^\delta}{J_n}\left(\sum_{f=1}^{3}\sum_{j=1}^{N_{fp}}\left[(\hat{\mathbf{f}}\cdot\hat{\mathbf{n}})_{f,j}^{\delta I}\right]\mathbf{h}_{f,j}\cdot\hat{\mathbf{n}}\right) d\mathbf{\Gamma}_S \\ &\quad= \int_{\mathbf{\Gamma}_n} u_n^\delta\left(n_x\{\{au_n^\delta\}\} + n_y\{\{bu_n^\delta\}\} + \frac{\lambda}{2}|an_x + bn_y|[\![u_n^\delta]\!]\right) d\mathbf{\Gamma}_n. \end{aligned}\tag{5.28}$$

Hence, from (5.27) and (5.28), equation (5.25) becomes

$$\begin{aligned}\int_{\mathbf{\Gamma}_n} u_n^\delta \left(\mathbf{f}_n^{\delta C}\cdot\mathbf{n}\right) d\mathbf{\Gamma}_n &= -\int_{\mathbf{\Gamma}_n} \left(a(u_n^\delta)^2 n_x + b(u_n^\delta)^2 n_y\right) d\mathbf{\Gamma}_n \\ &\quad + \int_{\mathbf{\Gamma}_n} u_n^\delta\left(n_x\{\{au_n^\delta\}\} + n_y\{\{bu_n^\delta\}\} + \frac{\lambda}{2}|an_x + bn_y|[\![u_n^\delta]\!]\right) d\mathbf{\Gamma}_n. \end{aligned}\tag{5.29}$$

Combining (5.21), (5.24) and (5.29) one obtains

$$\frac{d}{dt}\|u^\delta\|_{p,2}^2 = \sum_{n=1}^{N}\left\{ -\int_{\mathbf{\Gamma}_n} \frac{(an_x + bn_y)}{2}(u_-^\delta)^2 d\mathbf{\Gamma}_n + \int_{\mathbf{\Gamma}_n} (an_x + bn_y)(u_-^\delta)^2 d\mathbf{\Gamma}_n \right.$$

$$- \int_{\mathbf{\Gamma}_n} \left[\frac{(an_x + bn_y)}{2} ((u_-^\delta)^2 + u_-^\delta u_+^\delta) + \frac{\lambda}{2} |an_x + bn_y| ((u_-^\delta)^2 - u_-^\delta u_+^\delta) \right] d\mathbf{\Gamma}_n \Bigg\}$$

$$= - \sum_{n=1}^{N} \int_{\mathbf{\Gamma}_n} \left[\frac{(an_x + bn_y)}{2} u_-^\delta u_+^\delta + \frac{\lambda}{2} |an_x + bn_y| ((u_-^\delta)^2 - u_-^\delta u_+^\delta) \right] d\mathbf{\Gamma}_n \quad (5.30)$$

where the subscript n on u^δ has been dropped for simplicity. Equation (5.30) can be rewritten as a sum over edges, instead of a sum over elements by collecting along each edge the contributions from its two adjoining elements. Using the notation u_R^δ and u_L^δ to define the approximate solution on each side of an edge, and assuming that the domain is periodic, (5.30) becomes

$$\frac{d}{dt} \|u^\delta\|_{p,2}^2 = - \sum_{e=1}^{N_{edges}} \left\{ \int_{\mathbf{\Gamma}_e} \frac{\lambda}{2} |an_x + bn_y| \left[(u_L^\delta)^2 - 2u_R^\delta u_L^\delta + (u_R^\delta)^2 \right]) d\mathbf{\Gamma}_e \right\}$$

$$= - \sum_{e=1}^{N_{edges}} \left\{ \int_{\mathbf{\Gamma}_e} \frac{\lambda}{2} |an_x + bn_y| (u_L^\delta - u_R^\delta)^2 d\mathbf{\Gamma}_e \right\} \quad (5.31)$$

where N_{edges} is the total number of edges in the mesh and $\mathbf{\Gamma}_e$ is used to represent edge e. Since $0 \leq \lambda \leq 1$, it can be concluded that

$$\frac{d}{dt} \|u^\delta\|_{p,2}^2 \leq 0. \quad (5.32)$$

The previous result guarantees stability of the approximate solution for all polynomial orders p, independently of the location of the solution and flux points. To summarize, stability for the linear advection equation on linear triangular elements is guaranteed provided that the following requirements are satisfied:

1. The correction functions $\mathbf{h}_{f,j}$ must satisfy (5.14) in order for (5.32) to be true.
2. The constants c_m must satisfy $0 \leq c_m < \infty$, for all m. This ensures that $\|u^\delta\|_{p,2}$ is a norm of the approximate solution u^δ, from which stability in any norm is guaranteed (due to equivalence of norms in a finite dimensional space).

5.2 Identification of the Correction Fields $\phi_{f,j}$

In the previous section, it was shown that if every correction function $\mathbf{h}_{f,j}$ (for $f = 1$ to 3 and $j = 1$ to N_{fp}) satisfies (5.14), energy stability of the scheme is guaranteed (for linear advection). In this section, the methodology used to enforce (5.14) is presented. The procedure allows to obtain the form of the correction fields $\phi_{f,j}$, which can then be used in (4.35) to update the approximate solution values $\hat{u}_i^\delta$. To begin, consider expanding the approximate solution $\hat{u}^\delta$ in terms of a basis set L_i that is orthonormal on the reference equilateral triangle $\mathbf{\Omega}_S$, as follows

$$\hat{u}^\delta = \sum_{i=1}^{N_p} \zeta_i L_i(\mathbf{r}), \quad (5.33)$$

where ζ_i are the expansion coefficients. Such an orthonormal basis can be obtained through a Gram-Schmidt process on the monomial basis and is often referred to as a Dubiner basis [8].

The basis polynomials L_i (for $i = 1$ to N_p) have the form

$$L_i(\mathbf{r}) = \frac{2}{3^{1/4}} Q_v(a) Q_w^{(2v+1,0)}(b)(1-b)^v \tag{5.34}$$

$$i = w + (p+1)v + 1 - \frac{v}{2}(v-1), \quad (v,w) \geq 0; \quad v + w \leq p$$

where

$$a = \frac{3r}{2 - \sqrt{3}s}, \qquad b = \frac{1}{3}(2\sqrt{3}s - 1) \tag{5.35}$$

and $Q_n^{(\alpha,\beta)}$ is the normalized n^{th} order Jacobi polynomial. As a convention, the basis polynomial L_1 is associated with $(v, w) = (0, 0)$.

Substituting (5.33) into (5.14), one obtains

$$\sum_{i=1}^{N_p} \zeta_i \sum_{m=1}^{p+1} c_m \left(D^{(m,p)} L_i\right)\left(D^{(m,p)} \phi_{f,j}\right) = \sum_{i=1}^{N_p} \zeta_i \int_{\mathbf{\Omega}_S} \mathbf{h}_{f,j} \cdot \nabla_{rs} L_i \, d\mathbf{\Omega}_S \tag{5.36}$$

which can be satisfied independently of the transformed approximate solution (defined by the coefficients ζ_i) provided that

$$\sum_{m=1}^{p+1} c_m \left(D^{(m,p)} L_i\right)\left(D^{(m,p)} \phi_{f,j}\right) = \int_{\mathbf{\Omega}_S} \mathbf{h}_{f,j} \cdot \nabla_{rs} L_i d\mathbf{\Omega}_S, \quad \forall i. \tag{5.37}$$

Because L_1 is a constant, $D^{(m,p)} L_1 = 0$ and $\nabla_{rs} L_1 = 0$, thus (5.37) is automatically satisfied for $i = 1$. Hence, for a particular correction function $\mathbf{h}_{f,j}$, (5.37) provides $(N_p - 1)$ conditions on $\mathbf{h}_{f,j}$. Furthermore, the requirement that each correction function $\mathbf{h}_{f,j}$ satisfies (4.24) yields another set of $3(p+1)$ conditions. This results in a total of $\frac{1}{2}(p+1)(p+8)-1$ conditions on $\mathbf{h}_{f,j}$ that must be satisfied to guarantee stability. Because each correction function $\mathbf{h}_{f,j}$ lies in the space $RT_p(\mathbf{\Omega}_S)$ of dimension $(p+1)(p+3)$, (4.24) and (5.37) are not sufficient to fully determine the form of $\mathbf{h}_{f,j}$, except for the case $p = 1$ (since $\frac{1}{2}(p+1)(p+8) - 1 \leq (p+1)(p+3)$ for $p \geq 1$). However, one should note that the FR scheme defined in (4.35) does not depend directly on the form of $\mathbf{h}_{f,j}$ but rather, on the form of its divergence $\phi_{f,j}$. With that in mind, integrating the right hand side of (5.37) by parts, one obtains

$$\sum_{m=1}^{p+1} c_m \left(D^{(m,p)} L_i\right)\left(D^{(m,p)} \phi_{f,j}\right) = -\int_{\mathbf{\Omega}_S} \phi_{f,j} L_i d\mathbf{\Omega}_S + \int_{\mathbf{\Gamma}_S} \left(\mathbf{h}_{f,j} \cdot \hat{\mathbf{n}}\right) L_i d\mathbf{\Gamma}_S, \tag{5.38}$$

for $1 \leq i \leq N_p$. Because $\phi_{f,j} \in P_p(\mathbf{\Omega}_S)$, it can be expanded as

$$\phi_{f,j} = \sum_{k=1}^{N_p} \sigma_k L_k(\mathbf{r}) \tag{5.39}$$

where σ_k are the expansion coefficients. Substituting (5.39) into (5.38), and using the orthonormal property of the basis polynomials L_i, one obtains

$$\sum_{k=1}^{N_p} \sigma_k \sum_{m=1}^{p+1} c_m \left(D^{(m,p)} L_i\right)\left(D^{(m,p)} L_k\right) = -\sigma_i + \int_{\mathbf{\Gamma}_S} \left(\mathbf{h}_{f,j} \cdot \hat{\mathbf{n}}\right) L_i d\mathbf{\Gamma}_S \tag{5.40}$$

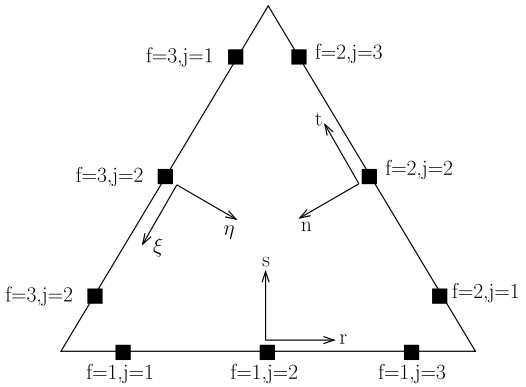

Fig. 5 Two rotated coordinate systems (n, t) and (ξ, η) associated with faces 2 and 3 of the reference equilateral triangle. Example shown corresponds to $p = 2$. Flux points are located at Gauss points along each edge

for $1 \leq i \leq N_p$. Since $\mathbf{h}_{f,j}$ lies in $RT_p(\mathbf{\Omega}_S)$, $\mathbf{h}_{f,j} \cdot \hat{\mathbf{n}}|_{\mathbf{\Gamma}_S}$ is a polynomial of degree p along each edge. Because its values are defined at $p + 1$ points along each edge (from (4.24)), the last term on the right hand side of (5.40) can be evaluated exactly. Therefore, (5.40) results in a system of N_p equations for N_p unknowns (the coefficients σ_k) which can be solved to obtain the form of each correction field $\phi_{f,j}$, and thereby guarantee that (5.14) is satisfied. Thus, by solving (5.40) for arbitrary values of the parameters c_m (within the range $0 \leq c_m < \infty$), one obtains an infinite range of energy stable FR schemes on triangular elements, defined by their correction fields $\phi_{f,j}$.

5.3 Enforcing Symmetry of the Correction Fields $\phi_{f,j}$

In the previous section, the methodology used to solve for the energy stable correction fields $\phi_{f,j}$ was presented. In addition to requiring stability of the scheme, it is also reasonable to demand that the correction fields $\phi_{f,j}$ satisfy the mirror and rotational symmetry conditions implied by the equilateral reference triangle $\mathbf{\Omega}_S$. Enforcing such conditions will ensure that for an initially symmetric solution $\hat{u}^\delta$ and symmetric numerical fluxes $(\hat{\mathbf{f}} \cdot \hat{\mathbf{n}})^{\delta I}_{f,j}$, the divergence of the correction flux $\nabla_{rs} \cdot \mathbf{f}^{\delta C}$ will also be symmetric. The two rotated coordinate systems (t, n) and (ξ, η) shown in Fig. 5 will be used to illustrate the symmetry requirements that the correction fields $\phi_{f,j}$ must satisfy.

For a pair of correction fields $\phi_{f,j}$ and ϕ_{f,j_2} such that $j_2 = p + 2 - j$ and for a single correction field associated with a flux point at the middle of an edge, mirror symmetry with respect to a line perpendicular to the edge, passing through its middle, is expected. For the case $p = 2$ illustrated in Fig. 5, this mirror symmetry requirement translates to

$$\phi_{1,2}(r, s) = \phi_{1,2}(-r, s), \qquad \phi_{1,1}(r, s) = \phi_{1,3}(-r, s), \tag{5.41}$$

$$\phi_{2,2}(t, n) = \phi_{2,2}(-t, n), \qquad \phi_{2,1}(t, n) = \phi_{2,3}(-t, n), \tag{5.42}$$

$$\phi_{3,2}(\xi, \eta) = \phi_{3,2}(-\xi, \eta), \qquad \phi_{3,1}(\xi, \eta) = \phi_{3,3}(-\xi, \eta). \tag{5.43}$$

Furthermore, rotational symmetry of the correction fields is expected. For $p = 2$, this translates to requiring that

$$\phi_{1,1}(r, s) = \phi_{2,1}(t, n) = \phi_{3,1}(\xi, \eta), \tag{5.44}$$

$$\phi_{1,2}(r, s) = \phi_{2,2}(t, n) = \phi_{3,2}(\xi, \eta), \tag{5.45}$$

$$\phi_{1,3}(r,s) = \phi_{2,3}(t,n) = \phi_{3,3}(\xi,\eta). \tag{5.46}$$

Similar symmetry requirements for arbitrary solution polynomial orders p can easily be obtained. It has been verified numerically that for arbitrary choices of the constants c_m, the correction fields $\phi_{f,j}$ obtained from the solution of the system given by (5.40) do not automatically satisfy the aforementioned symmetry requirements. However, for orders $p = 1$ to 6, it has been shown using the mathematical software Maple that solving (5.40) with the choice

$$c_m = \binom{p}{m-1} c = \frac{p!}{(m-1)!(p-m+1)!} c \tag{5.47}$$

for an arbitrary constant c, results in a set of correction fields $\phi_{f,j}$ that satisfy both the mirror symmetry and rotational symmetry requirements previously stated. The coefficients c_m are the binomial coefficients, scaled by a single scalar c. For that particular choice of the coefficients c_m, (5.37) becomes

$$c \sum_{m=1}^{p+1} \binom{p}{m-1} \left(D^{(m,p)} L_i\right) \left(D^{(m,p)} \phi_{f,j}\right) = \int_{\mathbf{\Omega}_S} \mathbf{h}_{f,j} \nabla_{rs} L_i \, d\mathbf{\Omega}_S, \quad \text{for } 1 \le i \le N_p \tag{5.48}$$

and (5.40) becomes

$$c \sum_{k=1}^{N_p} \sigma_k \sum_{m=1}^{p+1} \binom{p}{m-1} \left(D^{(m,p)} L_i\right) \left(D^{(m,p)} L_k\right) = -\sigma_i + \int_{\mathbf{\Gamma}_S} \left(\mathbf{h}_{f,j} \cdot \hat{\mathbf{n}}\right) L_i \, d\Gamma \tag{5.49}$$

for $1 \le i \le N_p$. The last equation can be used to solve for the coefficients σ_k (for $k = 1$ to N_p) of each correction field $\phi_{f,j}$. The correction fields thereby obtained result in energy stable FR schemes on triangles parameterized by a single scalar parameter c. Stability is guaranteed (for linear advection) in the norm,

$$\left[\sum_{n=1}^{N} \int_{\mathbf{\Omega}_n} \left(\frac{(u_n^\delta)^2}{2} + \frac{c}{2A_S} \sum_{m=1}^{p+1} \binom{p}{m-1} \left(D^{(m,p)} u_n^\delta\right)^2 \right) d\mathbf{\Omega}_n \right]^{1/2} \tag{5.50}$$

provided $0 \le c < \infty$. Furthermore, the correction fields $\phi_{f,j}$ obtained from the solution of the system of equations given by (5.49) are guaranteed to satisfy the mirror and rotational symmetry requirements on the reference equilateral triangle $\mathbf{\Omega}_S$. Because of the similarity between the 1D VCJH schemes and the energy stable FR schemes on triangles described in the previous sections, the latter will henceforth be referred as VCJH schemes on triangles.

5.4 Recovery of a Collocation Based Discontinuous Galerkin Scheme

In this section, it is shown that the VCJH scheme on triangles corresponding to a value of $c = 0$ recovers a collocation based nodal DG scheme such as the ones described in the textbook by Hesthaven and Warburton [9].

In a nodal DG method, the approximate solution $\hat{u}^\delta$ within the reference element $\mathbf{\Omega}_S$ is represented as in (4.17) and is required to satisfy

$$\int_{\mathbf{\Omega}_S} \frac{\partial \hat{u}^\delta}{\partial t} l_k \, d\mathbf{\Omega}_S = -\int_{\mathbf{\Omega}_S} \left(\nabla_{rs} \cdot \hat{\mathbf{f}}^\delta\right) l_k \, d\mathbf{\Omega}_S - \int_{\mathbf{\Gamma}_S} l_k \left[\left(\hat{\mathbf{f}}^\delta \cdot \hat{\mathbf{n}}\right) - \left(\hat{\mathbf{f}} \cdot \hat{\mathbf{n}}\right)^{\delta I} \right] d\mathbf{\Gamma}_S, \tag{5.51}$$

for all multi-dimensional Lagrange polynomials l_k associated with a set of N_p collocation points. In order to evaluate the volume and surface integrals in (5.51), an approximation must be made. In a collocation based nodal DG method, the approximate flux $\hat{\mathbf{f}}^{\delta}$ is obtained from

$$\hat{\mathbf{f}}^{\delta} = \hat{\mathbf{f}}^{\delta D} = \sum_{i=1}^{N_p} \hat{\mathbf{f}}_i^{\delta D} l_i \tag{5.52}$$

where the values of $\hat{\mathbf{f}}_i^{\delta D}$ are the values of the approximate flux evaluated directly at the collocation points. Furthermore, along each edge of the element, the difference between the normal transformed numerical flux $(\hat{\mathbf{f}} \cdot \hat{\mathbf{n}})^{\delta I}$ and the normal approximate flux $(\hat{\mathbf{f}}^{\delta D} \cdot \hat{\mathbf{n}})$ on $\mathbf{\Gamma}_S$ is approximated by a polynomial in $R_p(\mathbf{\Gamma}_S)$ whose form is determined by its values at a set of $p+1$ flux points along each edge. In other words, in a collocation based nodal DG approach

$$\left[(\hat{\mathbf{f}}^{\delta D} \cdot \hat{\mathbf{n}}) - (\hat{\mathbf{f}} \cdot \hat{\mathbf{n}})^{\delta I} \right] \Big|_{\mathbf{\Gamma}_S} \tag{5.53}$$

is approximated by

$$\sum_{f=1}^{3} \sum_{j=1}^{p+1} \left[(\hat{\mathbf{f}}^{\delta D} \cdot \hat{\mathbf{n}}) - (\hat{\mathbf{f}} \cdot \hat{\mathbf{n}})^{\delta I} \right]_{f,j} l_{f,j}^{1D} \tag{5.54}$$

where $l_{f,j}^{1D} \in R_p(\mathbf{\Gamma}_S)$ satisfies (4.29). Hence the approximate solution $\hat{u}^{\delta}$ in a collocation based nodal DG scheme satisfies

$$\begin{aligned} \int_{\mathbf{\Omega}_S} \frac{\partial \hat{u}^{\delta}}{\partial t} l_k \, d\mathbf{\Omega}_S = &- \int_{\mathbf{\Omega}_S} \left(\nabla_{rs} \cdot \hat{\mathbf{f}}^{\delta D} \right) l_k \, d\mathbf{\Omega}_S \\ &- \int_{\mathbf{\Gamma}_S} l_k \sum_{f=1}^{3} \sum_{j=1}^{p+1} \left[(\hat{\mathbf{f}}^{\delta D} \cdot \hat{\mathbf{n}}) - (\hat{\mathbf{f}} \cdot \hat{\mathbf{n}})^{\delta I} \right]_{f,j} l_{f,j}^{1D} d\mathbf{\Gamma}_S, \end{aligned} \tag{5.55}$$

for $k = 1$ to N_p.

For the VCJH schemes on triangles, (5.4) is used to update the approximate solution in time. On multiplying (5.4) by an arbitrary test function $\varphi \in P_p(\mathbf{\Omega}_S)$, and integrating over the reference element $\mathbf{\Omega}_S$, one obtains

$$\int_{\mathbf{\Omega}_S} \frac{\partial \hat{u}^{\delta}}{\partial t} \varphi \, d\mathbf{\Omega}_S = - \int_{\mathbf{\Omega}_S} \left(\nabla_{rs} \cdot \hat{\mathbf{f}}^{\delta D} \right) \varphi \, d\mathbf{\Omega}_S - \int_{\mathbf{\Omega}_S} \left(\nabla_{rs} \cdot \hat{\mathbf{f}}^{\delta C} \right) \varphi \, d\mathbf{\Omega}_S. \tag{5.56}$$

On integrating the last term on the right hand side of (5.56) by parts, one obtains

$$\int_{\mathbf{\Omega}_S} \frac{\partial \hat{u}^{\delta}}{\partial t} \varphi \, d\mathbf{\Omega}_S = - \int_{\mathbf{\Omega}_S} \left(\nabla_{rs} \cdot \hat{\mathbf{f}}^{\delta D} \right) \varphi \, d\mathbf{\Omega}_S - \int_{\mathbf{\Gamma}_S} \varphi \left(\hat{\mathbf{f}}^{\delta C} \cdot \hat{\mathbf{n}} \right) d\mathbf{\Gamma}_S + \int_{\mathbf{\Omega}_S} \hat{\mathbf{f}}^{\delta C} \cdot \nabla_{rs} \varphi \, d\mathbf{\Omega}_S. \tag{5.57}$$

The VCJH schemes on triangles are parameterized by a single parameter c and are obtained by enforcing (5.48). If $c = 0$, (5.48) simplifies to

$$\int_{\mathbf{\Omega}_S} \mathbf{h}_{f,j} \, \nabla_{rs} L_i \, d\mathbf{\Omega}_S = 0, \quad \forall i \text{ and } \forall f, j. \tag{5.58}$$

Because $\hat{\mathbf{f}}^{\delta C}$ is a linear combination of the correction functions $\mathbf{h}_{f,j}$ and any test function $\varphi \in P_p(\mathbf{\Omega}_S)$ can be written as a linear combination of the orthonormal basis polynomials $L_i \in P_p(\mathbf{\Omega}_S)$, it follows that if $c = 0$,

$$\int_{\mathbf{\Omega}_S} \hat{\mathbf{f}}^{\delta C} \nabla_{rs} \varphi \, d\mathbf{\Omega}_S = 0. \tag{5.59}$$

Therefore, (5.57) becomes

$$\int_{\mathbf{\Omega}_S} \frac{\partial \hat{u}^{\delta}}{\partial t} \varphi \, d\mathbf{\Omega}_S = -\int_{\mathbf{\Omega}_S} \left(\nabla_{rs} \cdot \hat{\mathbf{f}}^{\delta D} \right) \varphi \, d\mathbf{\Omega}_S - \int_{\mathbf{\Gamma}_S} \varphi \left(\hat{\mathbf{f}}^{\delta C} \cdot \hat{\mathbf{n}} \right) d\mathbf{\Gamma}_S. \tag{5.60}$$

Using (4.30), the integral over $\mathbf{\Gamma}_S$ can be written as

$$\int_{\mathbf{\Gamma}_S} \varphi \left(\hat{\mathbf{f}}^{\delta C} \cdot \hat{\mathbf{n}} \right) d\mathbf{\Gamma}_S = \int_{\mathbf{\Gamma}_S} \varphi \sum_{f=1}^{3} \sum_{j=1}^{N_{fp}} \Delta_{f,j} l_{f,j}^{1D} d\mathbf{\Gamma}_S. \tag{5.61}$$

Hence, the approximate solution for the VCJH scheme on triangles corresponding to $c = 0$ satisfies

$$\int_{\mathbf{\Omega}_S} \frac{\partial \hat{u}^{\delta}}{\partial t} \varphi \, d\mathbf{\Omega}_S = -\int_{\mathbf{\Omega}_S} \left(\nabla_{rs} \cdot \hat{\mathbf{f}}^{\delta D} \right) \varphi \, d\mathbf{\Omega}_S - \int_{\mathbf{\Gamma}_S} \varphi \sum_{f=1}^{3} \sum_{j=1}^{N_{fp}} \Delta_{f,j} l_{f,j}^{1D} d\mathbf{\Gamma}_f. \tag{5.62}$$

Because (5.62) is true for any $\varphi \in P_p(\mathbf{\Omega}_S)$, it follows that

$$\int_{\mathbf{\Omega}_S} \frac{\partial \hat{u}^{\delta}}{\partial t} l_k \, d\mathbf{\Omega}_S = -\int_{\mathbf{\Omega}_S} \left(\nabla_{rs} \cdot \hat{\mathbf{f}}^{\delta D} \right) l_k \, d\mathbf{\Omega}_S - \int_{\mathbf{\Gamma}_S} l_k \sum_{f=1}^{3} \sum_{j=1}^{N_{fp}} \Delta_{f,j} l_{f,j}^{1D} d\mathbf{\Gamma}_f \tag{5.63}$$

for all multi-dimensional Lagrange polynomial l_k of order p associated with the solution points. Equation (5.63) is the same as (5.55) provided that the solution and flux points in the VCJH scheme are located at the same location as the collocation and flux points in the collocation based nodal DG scheme. Therefore, it can be deduced that the approximate solution for a collocation based DG scheme is identical to the approximate solution for the VCJH scheme on triangles with $c = 0$.

6 Von Neumann Stability Analysis of the Vincent-Castonguay-Jameson-Huynh Schemes on Triangles

In this section, a von Neumann stability analysis of VCJH schemes on triangles is performed. The analysis is similar to the ones conducted by Van den Abeele to investigate the stability of the SD method [21], by Zhang and Shu [25] to study the dissipative properties of the DG method and by Kannan and Wang [13, 14] to investigate the linear stability of SV methods. The results of this section indicate how explicit time-step limits vary across the range of schemes and are used to identify values of c leading to schemes with increasing time-step limits (compared to the collocation based nodal DG schemes).

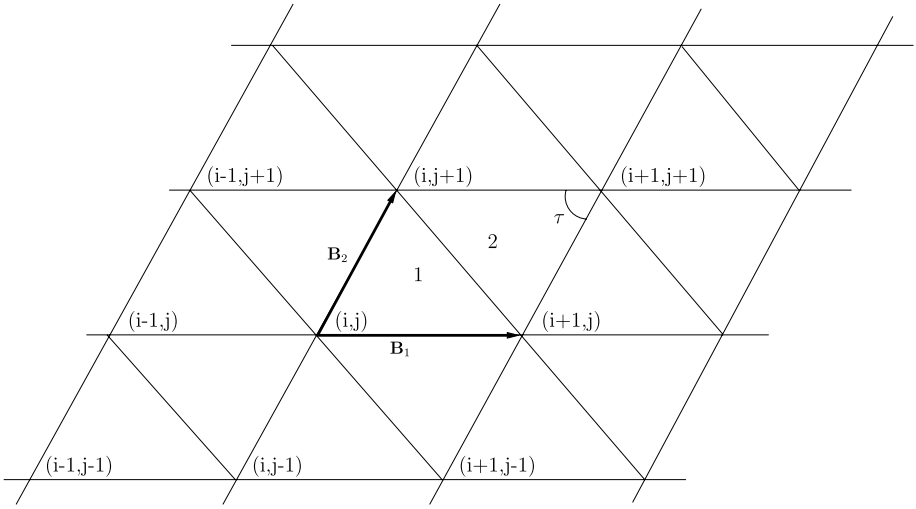

Fig. 6 Mesh generating pattern defined by the vectors $\mathbf{B}_1$ and $\mathbf{B}_2$

6.1 Theory

Consider the 2D linear advection equation

$$\frac{\partial u}{\partial t} + \nabla_{xy} \cdot (\mathbf{a}u) = 0 \tag{6.1}$$

where $\mathbf{a} = \|\mathbf{a}\|(\cos\psi, \sin\psi)$ and $u = u(x, y, t)$ is the conserved quantity. Let the computational domain $\boldsymbol{\Omega}$ be partitioned by repeating a grid generation pattern, as shown in Fig. 6.

The generating pattern is defined by the two vectors $\mathbf{B}_1 = (B_{1x}, B_{1y})$ and $\mathbf{B}_2 = (B_{2x}, B_{2y})$. The vector $\mathbf{B}_1$ is chosen to be horizontal with length ΔB, hence $\mathbf{B}_1 = (\Delta B, 0)$. The vector $\mathbf{B}_2$ also has length ΔB and is oriented at an angle τ with respect the x-coordinate direction, hence $\mathbf{B}_2 = \Delta B(\cos\tau, \sin\tau)$. Upon discretization of (6.1) using a VCJH scheme on triangles, and using the numerical flux defined by (5.22), one obtains the semi-discrete equation

$$\frac{d}{dt}\mathbf{U}_{i,j} = \frac{\|\mathbf{a}\|}{\Delta B}\left[\mathbf{A}\mathbf{U}_{i,j} + \mathbf{B}\mathbf{U}_{i-1,j} + \mathbf{C}\mathbf{U}_{i+1,j} + \mathbf{D}\mathbf{U}_{i,j-1} + \mathbf{E}\mathbf{U}_{i,j+1}\right] \tag{6.2}$$

where $\mathbf{U}_{i,j}$ is a vector of size $2N_p$ containing the unknown solution values for both triangular elements in the generating pattern (i, j) (refer to Fig. 6). The matrices $\mathbf{A}, \mathbf{B}, \mathbf{C}, \mathbf{D}$ and $\mathbf{E}$ are a function of the wave propagation direction ψ, the angle τ that defines the generating pattern, the parameter λ in the numerical flux definition and the scalar coefficient c by which the VCJH schemes on triangles are defined. Their formulation has been omitted for brevity. Following the methodology of the classic von Neumann stability analysis, a solution of the form

$$\mathbf{U}_{i,j} = \tilde{\mathbf{U}} \exp\left[\Im\kappa\left((iB_{1x} + jB_{2x})\cos\theta + (iB_{1y} + jB_{2y})\sin\theta\right)\right] \tag{6.3}$$

is sought for, where κ is the wave number of the harmonic plane wave, θ is the orientation angle of the harmonic plane wave, $\tilde{\mathbf{U}}$ is a complex vector of dimension $2N_p$ independent of

i and j and $\Im$ is the complex number $\sqrt{-1}$. Substituting (6.3) into the semi-discrete (6.2) and assuming periodic boundary conditions, one obtains

$$\frac{d}{dt}\tilde{\mathbf{U}} = \mathbf{L}\tilde{\mathbf{U}} \tag{6.4}$$

where the matrix $\mathbf{L}$, which is the spatial operator of the VCJH schemes on triangles, is defined as

$$\begin{aligned}\mathbf{L} = \frac{\|\mathbf{a}\|}{\Delta B}\Big\{&\mathbf{A} + \mathbf{B}\exp[-\Im\kappa(B_{1x}\cos\theta + B_{1y}\sin\theta)]\\ &+ \mathbf{C}\exp[\Im\kappa(B_{1x}\cos\theta + B_{1y}\sin\theta)]\\ &+ \mathbf{D}\exp[-\Im\kappa(B_{2x}\cos\theta + B_{2y}\sin\theta)]\\ &+ \mathbf{E}\exp[\Im\kappa(B_{2x}\cos\theta + B_{2y}\sin\theta)]\Big\}.\end{aligned} \tag{6.5}$$

Defining the non-dimensional quantities $\mathbf{B}_1'$, $\mathbf{B}_2'$ and K as $\mathbf{B}_1' = \mathbf{B}_1/\Delta B$, $\mathbf{B}_2' = \mathbf{B}_2/\Delta B$ and $K = \kappa\Delta B$, the matrix $\mathbf{L}$ can be rewritten as

$$\begin{aligned}\mathbf{L} = \frac{\|\mathbf{a}\|}{\Delta B}\Big\{&\mathbf{A} + \mathbf{B}\exp[-\Im K(B_{1x}'\cos\theta + B_{1y}'\sin\theta)]\\ &+ \mathbf{C}\exp[\Im K(B_{1x}'\cos\theta + B_{1y}'\sin\theta)]\\ &+ \mathbf{D}\exp[-\Im K(B_{2x}'\cos\theta + B_{2y}'\sin\theta)]\\ &+ \mathbf{E}\exp[\Im K(B_{2x}'\cos\theta + B_{2y}'\sin\theta)]\Big\}.\end{aligned} \tag{6.6}$$

Furthermore, defining the non-dimensional time $t' = t\frac{\Delta B}{\|\mathbf{a}\|}$, (6.4) becomes

$$\frac{d}{dt'}\tilde{\mathbf{U}} = \mathbf{L}'\tilde{\mathbf{U}} \tag{6.7}$$

where

$$\mathbf{L}' = \mathbf{L}\frac{\Delta B}{\|\mathbf{a}\|}. \tag{6.8}$$

The matrix $\mathbf{L}'$ depends on the following parameters: the non-dimensional wave number K, the wave propagation direction ψ, the harmonic plane orientation θ, the angle τ that defines the generating pattern, the parameter λ in the numerical flux definition and the scalar coefficient c by which VCJH schemes are defined. For a given explicit time discretization method (such as forward Euler or an explicit Runge-Kutta scheme), the semi-discrete equation (6.7) can be written in the form

$$\tilde{\mathbf{U}}^{m+1} = \mathbf{M}\tilde{\mathbf{U}}^{m} \tag{6.9}$$

where $\tilde{\mathbf{U}}^m$ is the solution at time level m and the matrix $\mathbf{M}$ depends on the spatial operator $\mathbf{L}'$ and the non-dimensional time step $\Delta t'$. The exact form of $\mathbf{M}$ for various time discretization methods will be given in the following subsection. To have a bounded numerical solution, the matrix $\mathbf{M}$ must have eigenvalues whose moduli are less than 1. Hence, for a particular spatial discretization operator $\mathbf{L}'$ and a time advancement scheme, one can identify the maximum value of the non-dimensional time step $\Delta t'$ that allows this condition to be satisfied.

6.2 Results

In the previous section, a semi-discrete form of the governing equation (6.7) was derived in which the spatial discrete operator $\mathbf{L}'$ is a function of the parameters $K, \psi, \tau, \theta, \lambda$ and c. In this section, the time-step limits for the fully discretized system given by (6.9) are computed for three different time advancement schemes, two different mesh generating pattern and for the range of values of c that satisfy $0 \leq c < \infty$ (which is the range that guarantees linear stability in the norm given by (5.50)). The analysis is performed for solution polynomials of order $p = 2$ to 4 and the upwind parameter λ is set to 1, thus recovering a fully upwind numerical flux. The two mesh generating patterns correspond to values τ of 60° and 90°. The time advancement schemes considered are the classic 3-stage, 3rd order Runge-Kutta scheme (denoted by RK33), the classic 4-stage, 4$^{\text{th}}$ order Runge-Kutta scheme (denoted by RK44) and the low-storage 5-stage, 4$^{\text{th}}$ order Runge-Kutta scheme [1] (denoted RK54). For the classic 3-stage, 3rd order Runge-Kutta scheme (RK33), the matrix $\mathbf{M}$ takes the form

$$\mathbf{M} = I + \Delta t' \mathbf{L}' + \frac{(\Delta t')^2}{2}(\mathbf{L}')^2 + \frac{(\Delta t')^3}{6}(\mathbf{L}')^3, \tag{6.10}$$

for the classic 4-stage, 4$^{\text{th}}$ order Runge-Kutta scheme (RK44)

$$\mathbf{M} = I + \Delta t' \mathbf{L}' + \frac{(\Delta t')^2}{2}(\mathbf{L}')^2 + \frac{(\Delta t')^3}{6}(\mathbf{L}')^3 + \frac{(\Delta t')^4}{24}(\mathbf{L}')^4, \tag{6.11}$$

and finally, for the low-storage 5-stage, 4$^{\text{th}}$-order Runge-Kutta scheme (RK54),

$$\mathbf{M} = I + \Delta t' \mathbf{L}' + \frac{(\Delta t')^2}{2}(\mathbf{L}')^2 + \frac{(\Delta t')^3}{6}(\mathbf{L}')^3 + \frac{(\Delta t')^4}{24}(\mathbf{L}')^4 + \frac{(\Delta t')^5}{200}(\mathbf{L}')^5. \tag{6.12}$$

For each combination of a time advancement scheme, mesh generating pattern and value of c, the eigenvalues of the matrix $\mathbf{M}$ are computed numerically at a discrete number of points for $K, \psi, \theta \in [0, 2\pi]$ for a given $\Delta t'$, which is increased incrementally until the stability condition is violated. From this analysis, plots of the maximum non-dimensional time step $\Delta t'$ versus the parameter c are obtained for the different time-advancement schemes. Results for $p = 2$ to 4 are shown in Figs. 7(a) to 7(f) for the mesh generating pattern with $\tau = 60°$ and in Figs. 8(a) to 8(f) for the mesh generating pattern with $\tau = 90°$. The c-axis is shown on both a logarithmic scale to show the behaviour over a wide range of values of c and a linear scale to provide more details in the regions of high gradients. For all orders p and for both mesh generating patterns, the maximum allowable time step $\Delta t'$ is positive for values of c in the range $0 \leq c < \infty$, confirming that the VCJH schemes on triangles are linearly stable. Furthermore, it is clear from those figures that there exists a value of c resulting in a maximal time-step limit. These values of c, henceforth referred as c_+, depend on the polynomial order, the mesh generating pattern and the time-advancement scheme. They are presented in Table 1. The VCJH schemes on triangles corresponding to c_+ allow a significant increase in the explicit time-step limits compared to the collocation based nodal DG method (recovered when $c = 0$). For example, for $p = 2$, the use of $c = c_+$ results in time-step limits at least two times bigger than those associated with $c = 0$.

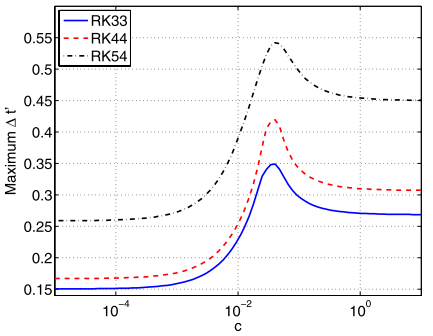

(a) $p = 2$, log scale

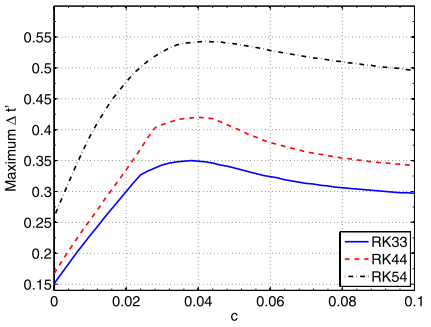

(b) $p = 2$, linear scale

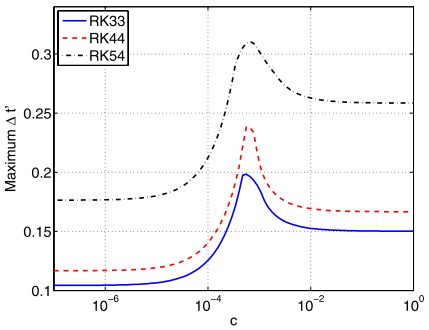

(c) $p = 3$, log scale

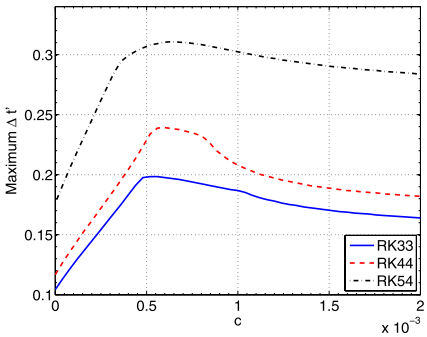

(d) $p = 3$, linear scale

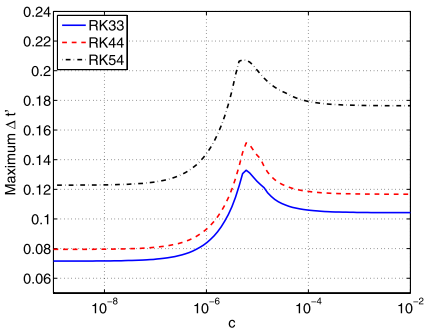

(e) $p = 4$, log scale

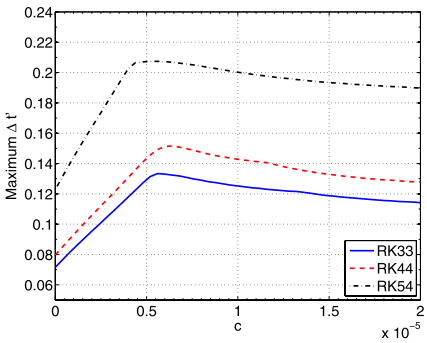

(f) $p = 4$, linear scale

Fig. 7 Plots of maximum non-dimensional time step versus parameter c for linear advection equation on triangular grid with $p = 2$ (**a**–**b**), $p = 3$ (**c**–**d**) and $p = 4$ (**e**–**f**). For all cases, a fully upwind flux was used and the angle τ used to prescribe the mesh generating pattern was set to 60°

7 Numerical Experiments

In this section, numerical experiments are performed on the two-dimensional linear advection equation

$$\frac{\partial u}{\partial t} = \frac{\partial u}{\partial x} + \frac{\partial u}{\partial y}, \tag{7.1}$$

Table 1 Values of c_+ for various polynomial orders p and time integration schemes

Polynomial degree	$\tau = 60°$			$\tau = 90°$		
p	RK33	RK44	RK54	RK33	RK44	RK54
2	3.8e-2	4.0e-2	4.3e-2	3.7e-2	4.1e-2	4.3e-2
3	5.4e-4	5.9e-4	6.4e-4	6.0e-4	6.0e-4	6.0e-4
4	5.6e-6	6.4e-6	5.3e-6	6.4e-6	6.4e-6	5.6e-6

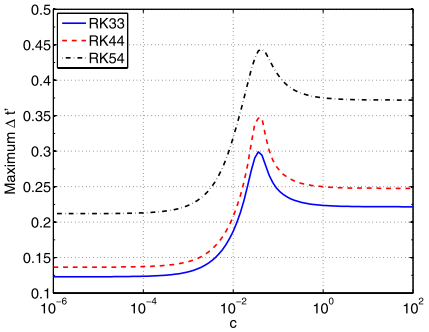

(a) $p = 2$, log scale

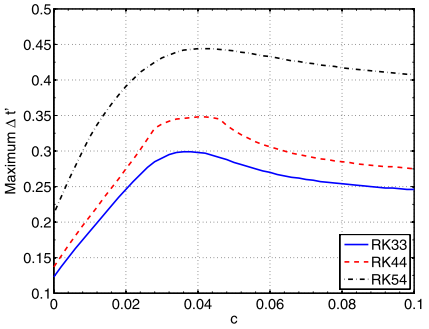

(b) $p = 2$, linear scale

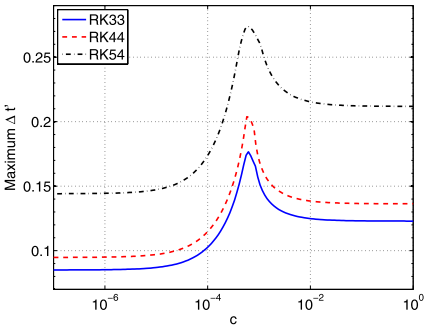

(c) $p = 3$, log scale

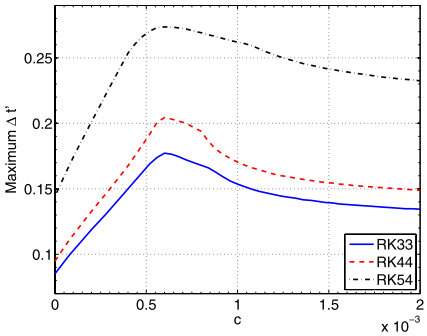

(d) $p = 3$, linear scale

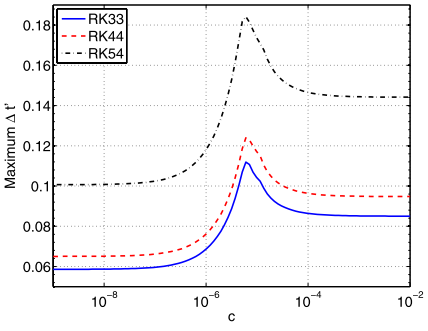

(e) $p = 4$, log scale

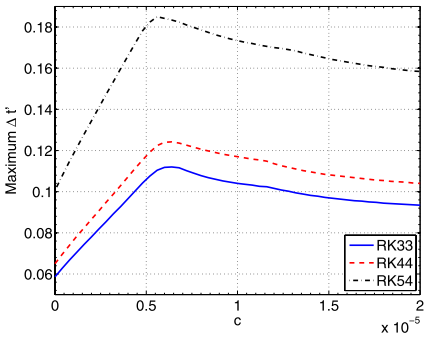

(f) $p = 4$, linear scale

Fig. 8 Plots of maximum non-dimensional time step versus parameter c for linear advection equation on triangular grid with $p = 2$ (**a**–**b**), $p = 3$ (**c**–**d**) and $p = 4$ (**e**–**f**). For all cases, a fully upwind flux was used and the angle τ used to prescribe the mesh generating pattern was set to 90°

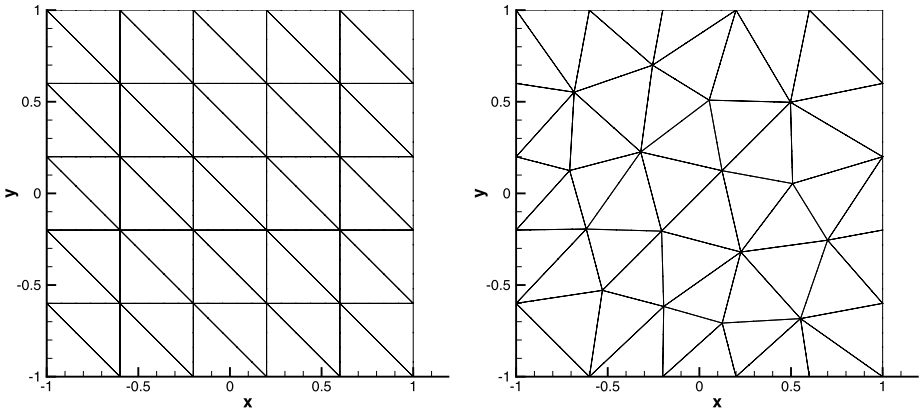

Fig. 9 Regular (**a**) and irregular (**b**) $5 \times 5 \times 2$ triangular grids used in numerical experiments

where $u = u(x, y, t)$ is the conserved scalar quantity. The numerical experiments are used to assess the order of accuracy of the new VCJH schemes on triangles and to verify the time-step limits obtained in the previous section. The computational domain is taken to be $-1 \leq x \leq 1, -1 \leq y \leq 1$ and periodic boundary conditions are used in both the x and y directions. The initial conditions is

$$u(x, y, 0) = \sin(\pi(x + y)). \tag{7.2}$$

Two types of grids are used: one regular, shown in Fig. 9(a), generated by repeating a generating pattern and one irregular, shown in Fig. 9(b).

To perform an order of accuracy study, each grid is repeatedly refined four times, by splitting each of its elements into four. Hence, the two sets of grids contain $N_x \times N_x \times 2$ cells with N_x taking the values of 5, 10, 20, 40 and 80 for the different refinement levels. For the test cases presented in this section, the low-storage 5-stage 4^{th} order Runge-Kutta scheme is used and the simulation is carried out until $t = 1$. In order to verify the accuracy of the schemes, the discrete L_2 error norm defined by

$$L_2 \text{ error } = \sqrt{\frac{\sum_{n=1}^{N} \sum_{i=1}^{N_p} (u_{i,n} - u_{i,n}^e)^2}{N \cdot N_p}} \tag{7.3}$$

is used, where N_p is the number of solution points per cell, N is the total number of cells and $u_{i,n}$ and $u_{i,n}^e$ are the approximate and exact solutions at solution point i of cell n, respectively. When conducting the order of accuracy study, the time step is chosen sufficiently small so that the error from the time discretization scheme is negligible compared to the spatial discretization error. Two different VCJH schemes on triangles corresponding to two different values of c are tested. In the first scheme, the parameter c is set to 0, thereby recovering a collocation based nodal DG scheme. For the second scheme, the values of c_+ from Table 1 for the low-storage 4^{th} order RK scheme and the mesh generating pattern $\tau = 90°$ are used. The corresponding values of c_+ are $4.3e^{-2}$, $6.0e^{-4}$ and $5.6e^{-6}$ for orders $p = 2, 3$ and 4 respectively. Furthermore, for each simulation, the maximum allowable non-dimensional

Table 2 Numerical results obtained on the regular grids for the advection equation, for various polynomial orders p and for two values of c

p	Grid Size	$c = 0$			$c = c_+$		
		L_2 error	Order	$\Delta t'_{max}$	L_2 error	Order	$\Delta t'_{max}$
2	$5 \times 5 \times 2$	1.415e-02	–	0.210	4.940e-02	–	0.442
	$10 \times 10 \times 2$	1.881e-03	2.91	0.210	7.170e-03	2.78	0.442
	$20 \times 20 \times 2$	2.379e-04	2.98	0.210	9.530e-04	2.91	0.442
	$40 \times 40 \times 2$	2.982e-05	3.00	0.210	1.216e-04	2.97	0.442
	$80 \times 80 \times 2$	3.730e-06	3.00	0.210	1.524e-05	3.00	0.440
3	$5 \times 5 \times 2$	1.167e-03	–	0.142	3.890e-03	–	0.272
	$10 \times 10 \times 2$	7.549e-05	3.95	0.142	2.464e-04	3.98	0.270
	$20 \times 20 \times 2$	4.939e-06	3.93	0.142	1.544e-05	4.00	0.270
	$40 \times 40 \times 2$	3.084e-07	4.00	0.142	9.652e-07	4.00	0.270
	$80 \times 80 \times 2$	1.928e-08	4.00	0.142	6.032e-08	4.00	0.270
4	$5 \times 5 \times 2$	8.324e-05	–	0.100	2.486e-04	–	0.182
	$10 \times 10 \times 2$	2.763e-06	4.91	0.100	8.375e-06	4.89	0.180
	$20 \times 20 \times 2$	8.697e-08	4.99	0.100	2.644e-07	4.99	0.180
	$40 \times 40 \times 2$	2.716e-09	5.00	0.100	8.347e-09	4.99	0.180

time step, $\Delta t'$, is determined numerically. The non-dimensional time step is defined as

$$\Delta t' = \frac{\|\mathbf{a}\|}{\Delta x} \Delta t \tag{7.4}$$

where $\|\mathbf{a}\|$ is the wave speed ($\|\mathbf{a}\| = \sqrt{2}$ for the current problem) and $\Delta x = \frac{2}{N_x}$. For each combination of p and grid size, the non-dimensional time step was increased by 2.0e-3 until the solution went unstable before reaching a time t of 100. Tables 2 and 3 present the computed errors and the maximum values of $\Delta t'$ on both grids for the two different VCJH schemes on triangles. For both values of c ($c = 0$ and $c = c_+$), the optimal order of accuracy is achieved ($(p+1)^{\text{th}}$ order of accuracy for degree p polynomial) for all polynomial orders p, although the nodal DG approach gives smaller errors. Furthermore, as expected from the von Neumann stability analysis, the VCJH schemes corresponding to values of c_+ allow a significantly larger explicit time-step compared to that of the collocation based nodal DG scheme. The maximum non-dimensional time steps computed in the numerical experiments on the regular grid fall within 2% of the value predicted from the von Neumann stability analysis.

8 Conclusions

In this article, a new extension of the FR approach to triangular elements has been proposed, and used to identify a new class of high-order linearly stable FR schemes on triangular elements. The schemes, referred to as VCJH schemes on triangles, are parameterized by a single scalar quantity c. The new approach provides a simple methodology to implement an infinite range of linearly stable FR schemes on triangular elements. Stability analysis of the schemes allows identification of values of c that lead to schemes with increased time-step limits (compared to the collocation based nodal DG method). Furthermore, the schemes with

Table 3 Numerical results obtained on the irregular grids for the advection equation, for various polynomial orders p and for two values of c

p	Grid Size	$c=0$			$c=c_+$		
		L_2 error	Order	$\Delta t'_{max}$	L_2 error	Order	$\Delta t'_{max}$
2	$5\times5\times2$	3.922e-02	–	0.288	1.362e-01	–	0.568
	$10\times10\times2$	5.336e-03	2.82	0.272	2.131e-02	2.68	0.558
	$20\times20\times2$	7.350e-04	2.91	0.262	2.947e-03	2.85	0.554
	$40\times40\times2$	8.997e-05	3.03	0.254	3.720e-04	2.99	0.522
	$80\times80\times2$	1.107e-05	3.02	0.250	4.660e-05	3.00	0.504
3	$5\times5\times2$	5.690e-03	–	0.190	1.605e-02	–	0.346
	$10\times10\times2$	3.094e-04	3.87	0.178	1.211e-03	3.73	0.336
	$20\times20\times2$	2.456e-05	3.99	0.168	7.809e-05	3.95	0.324
	$40\times40\times2$	1.523e-06	4.01	0.160	4.910e-06	3.99	0.316
	$80\times80\times2$	9.519e-08	4.00	0.150	3.069e-07	4.00	0.308
4	$5\times5\times2$	6.801e-04	–	0.136	1.842e-03	–	0.232
	$10\times10\times2$	2.066e-05	5.04	0.130	5.424e-05	5.09	0.224
	$20\times20\times2$	6.982e-07	4.89	0.124	1.803e-06	4.91	0.216
	$40\times40\times2$	2.128e-08	5.04	0.120	5.449e-08	5.05	0.212

increased time-step limits have been shown, in numerical experiments, to yield the optimal order of accuracy for the linear advection problem. The new VCJH schemes on triangles represent an important extension of the 1D VCJH schemes because triangular elements are essential for the simulation of two dimensional flows over complex geometries. Future studies will investigate how stability and accuracy depend on c for non-linear problems and extend the methodology to simplex elements in 3D.

Acknowledgements The authors would like to thank the Natural Sciences and Engineering Research Council of Canada, the Fonds de Recherche sur la Nature et les Technologies du Québec, the Stanford Graduate Fellowship Program, the National Science Foundation (grants 0708071 and 0915006) and the Air Force Office of Scientific Research (grants FA9550-07-1-0195 and FA9550-10-1-0418) for supporting this work.

Appendix: Raviart-Thomas Space

In this section, a brief introduction to the Raviart-Thomas space is presented. The Raviart-Thomas space was originally introduced in 1977 [18] to approximate the space H(div).

For the reference triangle $\mathbf{\Omega}_S$, the Raviart-Thomas space is defined as

$$RT_p(\mathbf{\Omega}_S) = (P_p(\mathbf{\Omega}_S))^2 + \mathbf{r}P_p(\mathbf{\Omega}_S) \tag{9.1}$$

where $\mathbf{r}=(r,s)$, $P_p(\mathbf{\Omega}_S)$ is the space of polynomials of degree at most p and $P_p(\mathbf{\Omega}_S)^2 = (P_p(\mathbf{\Omega}_S), P_p(\mathbf{\Omega}_S))$ (the 2-dimensional vector space for which each component is a polynomial of degree at most p). The dimension of $P_p(\mathbf{\Omega}_S)$ is $\frac{1}{2}(p+1)(p+2)$ while the dimension of $RT_p(\mathbf{\Omega}_S)$ is $(p+1)(p+3)$. The space $RT_p(\mathbf{\Omega}_S)$ has two important properties.

Property 1

Because $RT_p(\mathbf{\Omega}_S) \subset (P_p(\mathbf{\Omega}_S))^2$, for $\mathbf{q} \in RT_p(\mathbf{\Omega}_S)$, the following property holds

$$\nabla \cdot \mathbf{q} \in P_p(\mathbf{\Omega}_S).$$

Property 2

Let the polynomial space $R_p(\mathbf{\Gamma}_S)$ be defined on the edges of the reference element as

$$R_p(\mathbf{\Gamma}_S) = \left\{\phi \mid \phi \in L^2(\mathbf{\Gamma}_S),\ \ \phi|_{\mathbf{\Gamma}_f} \in P_p(\mathbf{\Gamma}_f),\ \ \forall \mathbf{\Gamma}_f\right\} \tag{9.2}$$

where $\mathbf{\Gamma}_f$ is used to represent edge f of the reference element $\mathbf{\Omega}_S$. Functions of $R_p(\mathbf{\Gamma}_S)$ are polynomials of degree $\leq p$ on each side of $\mathbf{\Omega}_S$, and are not necessarily continuous at the vertices. For $\mathbf{q} \in RT_P(\mathbf{\Omega}_S)$, the following property holds

$$\mathbf{q} \cdot \hat{\mathbf{n}}\big|_{\mathbf{\Gamma}_S} \in R_p(\mathbf{\Gamma}_S). \tag{9.3}$$

This can be proved as follows. Let $\mathbf{q} \in RT_p(\mathbf{\Omega}_S)$ which can be written as $\mathbf{q} = \mathbf{q}_0 + \mathbf{r}q_p$ where $\mathbf{q}_0 \in (P_p(\mathbf{\Omega}_S))^2$ and $q_p \in P_p(\mathbf{\Omega}_S)$. Also, let the $\hat{\mathbf{n}} = (n_r, n_s)$ be the normal to a side of the reference triangle $\mathbf{\Omega}_S$. Then we have

$$\mathbf{q} \cdot \hat{\mathbf{n}} = \mathbf{q}_0 \cdot \hat{\mathbf{n}} + q_p(rn_r + sn_s). \tag{9.4}$$

On a side of $\mathbf{\Omega}_S$, $(rn_r + sn_s)$ is a constant, and therefore $\mathbf{q} \cdot \hat{\mathbf{n}}$ is a polynomial of degree p.

Examples of Elements of $RT_p(\Omega_S)$

Let $\mathbf{q} = (q_r, q_s)$ be an element of $RT_p(\mathbf{\Omega}_S)$. Then $\mathbf{q}$ takes the following form for $p = 2, 3$ and 4.

$p = 2$

$$\begin{aligned} q_r(r,s) &= a_1 + c_1 r \\ q_s(r,s) &= b_1 + c_1 s \end{aligned}$$

$p = 3$

$$\begin{aligned} q_r(r,s) &= a_1 + a_2 r + a_3 s + c_1 r^2 + c_2 rs \\ q_s(r,s) &= b_1 + b_2 r + b_3 s + c_1 rs + c_2 s^2 \end{aligned}$$

$p = 4$

$$\begin{aligned} q_r(r,s) &= a_1 + a_2 r + a_3 s + a_4 r^2 + a_5 rs + a_6 s^2 + c_1 r^3 + c_2 r^2 s + c_3 rs^2 \\ q_s(r,s) &= b_1 + b_2 r + b_3 s + b_4 r^2 + b_5 rs + b_6 s^2 + c_1 r^2 s + c_2 rs^2 + c_3 s^3 \end{aligned}$$

References

1. Carpenter, M.H., Kennedy, C.: Fourth-order 2n-storage Runge-Kutta schemes. Technical Report TM 109112, NASA, NASA Langley Research Center (1994)

2. Castonguay, P., Liang, C., Jameson, A.: Simulation of transitional flow over airfoils using the spectral difference method. In: 40th AIAA Fluid Dynamics Conference, Chicago, IL, June 28–July 1 (2010). AIAA Paper, 2010-4626
3. Cockburn, B., Shu, C.W.: TVB Runge-Kutta local projection discontinuous Galerkin finite element method for conservation laws II: general framework. Math. Comput. **52**(186), 411–435 (1989)
4. Cockburn, B., Shu, C.W.: The Runge-Kutta local projection P1-discontinuous Galerkin finite element method for scalar conservation laws. RAIRO Modél. Math. Anal. Numér. **25**(3), 337–361 (1991)
5. Cockburn, B., Shu, C.W.: Runge-Kutta discontinuous Galerkin methods for convection-dominated problems. J. Sci. Comput. **16**(3), 173–261 (2001)
6. Cockburn, B., Lin, S.Y., Shu, C.W.: TVB Runge-Kutta local projection discontinuous Galerkin finite element method for conservation laws III: one-dimensional systems. J. Comput. Phys. **84**(1), 90–113 (1989)
7. Cockburn, B., Hou, S., Shu, C.W.: The Runge-Kutta local projection discontinuous Galerkin finite element method for conservation laws. IV: The multidimensional case. Math. Comput. **54**(190), 545–581 (1990)
8. Dubiner, M.: Spectral methods on triangles and other domains. J. Sci. Comput. **6**(4), 345–390 (1991)
9. Hesthaven, J.S., Warburton, T.: Nodal Discontinuous Galerkin Methods: Algorithms, Analysis, and Applications. Springer, Berlin (2007)
10. Huynh, H.T.: A flux reconstruction approach to high-order schemes including discontinuous Galerkin methods. In: 18th AIAA Computational Fluid Dynamics Conference, Miami, FL, Jun 25–28 (2007). AIAA Paper, 4079
11. Huynh, H.T.: A reconstruction approach to high-order schemes including discontinuous Galerkin for diffusion. In: 47th AIAA Aerospace Sciences Meeting, Orlando, FL, Jan 5–8 (2009). AIAA Paper, 403
12. Jameson, A.: A proof the stability of the spectral difference method for all orders of accuracy. J. Sci. Comput. **45**(1–3), 348–358 (2010)
13. Kannan, R., Wang, Z.J.: A study of viscous flux formulations for a p-multigrid spectral volume Navier Stokes solver. J. Sci. Comput. **41**(2), 165–199 (2009)
14. Kannan, R., Wang, Z.J.: LDG2: A variant of the LDG flux formulation for the spectral volume method. J. Sci. Comput. **46**(2), 314–328 (2011)
15. Kopriva, D.A., Kolias, J.H.: A conservative staggered-grid Chebyshev multidomain method for compressible flows. J. Comput. Phys. **125**, 244–261 (1996)
16. Liang, C., Kannan, R., Wang, Z.J.: A p-multigrid spectral difference method with explicit and implicit smoothers on unstructured triangular grids. Comput. Fluids **38**, 254–265 (2009)
17. Liu, Y., Vinokur, M., Wang, Z.J.: Spectral difference method for unstructured grids i: Basic formulation. J. Comput. Phys. **216**, 780–801 (2006)
18. Raviart, P.A., Thomas, J.M.: A mixed hybrid finite element method for the second order elliptic problems. In: Mathematical Aspects of the Finite Element Method. Lectures Notes in Mathematics. Springer, Berlin (1977)
19. Reed, W.H., Hill, T.R.: Triangular mesh methods for the neutron transport equation. Los Alamos Report LA-UR-73-479 (1973)
20. Roe, P.L.: Approximate Riemann solvers, parameter vectors and difference schemes. J. Comput. Phys. **43**, 357–372 (1981)
21. Van den Abeele, K., Lacor, C., Wang, Z.J.: On the stability and accuracy of the spectral difference method. J. Sci. Comput. **37**(2), 162–188 (2008)
22. Vincent, P.E., Castonguay, P., Jameson, A.: A new class of high-order energy stable flux reconstruction schemes. J. Sci. Comput. **47**(1), 50–72 (2011)
23. Wang, Z.J., Gao, H.: A unifying lifting collocation penalty formulation including the discontinuous Galerkin, spectral volume/difference methods for conservation laws on mixed grids. J. Comput. Phys. **228**(21), 8161–8186 (2009)
24. Wang, Z.J., Liu, Y., May, G., Jameson, A.: Spectral difference method for unstructured grids II: Extension to the Euler equations. J. Sci. Comput. **32**, 45–71 (2007)
25. Zhang, M., Shu, C.W.: An analysis of three different formulations of the discontinuous Galerkin method for diffusion equations. Math. Models Methods Appl. Sci. **13**(3), 395–414 (2003)